Available online at www.sciencedirect.com
SCIENCE DIRECT®
Geochimica et Cosmochimica Acta 70 (2006) 2510–2529
Geochimica
www.elsevier.com/locate/gca

Preferential formation of ^{13}C–^{18}O bonds in carbonate minerals, estimated using first-principles lattice dynamics

Edwin A. Schauble [a,*], Prosenjit Ghosh [b], John M. Eiler [b]

[a] Department of Earth and Space Sciences, University of California, Los Angeles, Box 951567, Los Angeles, CA 90095-1567, USA
[b] Division of Geological and Planetary Sciences, California Institute of Technology, MC 100-23, Pasadena, CA 91125, USA

Received 2 September 2005; accepted in revised form 3 February 2006

Abstract

Equilibrium constants for internal isotopic exchange reactions of the type:

$$Ca^{12}C^{18}O^{16}O_2 + Ca^{13}C^{16}O_3 \leftrightarrow Ca^{13}C^{18}O^{16}O_2 + Ca^{12}C^{16}O_3$$

for individual CO_3^{2-} groups in the carbonate minerals calcite ($CaCO_3$), aragonite ($CaCO_3$), dolomite ($CaMg(CO_3)_2$), magnesite ($MgCO_3$), witherite ($BaCO_3$), and nahcolite ($NaHCO_3$) are calculated using first-principles lattice dynamics. Calculations rely on density functional perturbation theory (DFPT) with norm-conserving planewave pseudopotentials to determine the vibrational frequencies of isotopically substituted crystals. Our results predict an ~0.4‰ excess of $^{13}C^{18}O^{16}O_2^{2-}$ groups in all studied carbonate minerals at room-temperature equilibrium, relative to what would be expected in a stochastic mixture of carbonate isotopologues with the same bulk $^{13}C/^{12}C$, $^{18}O/^{16}O$, and $^{17}O/^{16}O$ ratios. The amount of excess $^{13}C^{18}O^{16}O_2^{2-}$ decreases with increasing temperature of equilibration, from 0.5‰ at 0 °C to <0.1‰ at 300 °C, suggesting that measurements of multiply substituted isotopologues of carbonate could be used to infer temperatures of ancient carbonate mineral precipitation and alteration events, even where the $\delta^{18}O$ of coexisting fluids is uncertain. The predicted temperature sensitivity of the equilibrium constant is ~0.003‰/°C at 25 °C. Estimated equilibrium constants for the formation of $^{13}C^{18}O^{16}O_2^{2-}$ are remarkably uniform for the variety of minerals studied, suggesting that temperature calibrations will also be applicable to carbonate minerals not studied here without greatly compromising accuracy. A related equilibrium constant for the reaction:

$$Ca^{12}C^{18}O^{16}O_2 + Ca^{12}C^{17}O^{16}O_2 \leftrightarrow Ca^{12}C^{18}O^{17}O^{16}O + Ca^{12}C^{16}O_3$$

in calcite indicates formation of 0.1‰ excess $^{12}C^{18}O^{17}O^{16}O^{2-}$ at 25 °C. In a conventional phosphoric acid reaction of carbonate to form CO_2 for mass-spectrometric analysis, molecules derived from $^{13}C^{18}O^{16}O_2^{2-}$ dominate (~96%) the mass 47 signal, and $^{12}C^{18}O^{17}O^{16}O^{2-}$ contributes most of the remainder (3%). This suggests that carbonate internal equilibration temperatures can be recovered from acid-generated CO_2 if abundances of isotopologues with mass 44–47 can be measured to sufficient precision. We have also calculated $^{18}O/^{16}O$ and $^{13}C/^{12}C$ reduced partition function ratios for carbonate minerals, and find them to be in good agreement with experiments and empirical calibrations. Carbon and oxygen isotope fractionation factors in hypothetical ^{40}Mg—magnesite and ^{40}Ba—witherite indicate that M^{2+}-cation mass does not contribute significantly to equilibrium isotopic fractionations between carbonate minerals.

1. Introduction

This study extends recent theoretical estimates and measurements of abundance variations of CO_2 molecules containing multiple heavy isotopes (e.g., $^{13}C^{18}O^{16}O$) (Wang et al., 2004; Eiler and Schauble, 2004; Affek and Eiler, 2006) to examine possible applications of $^{13}C^{18}O^{16}O_2^{2-}$ abundance measurements in carbonate minerals. Carbonate minerals, unlike CO_2, are likely to retain isotopic signatures over geologic time, and therefore have the potential to provide information about ancient environments.

* Corresponding author. Fax: +1 310 825 2779.
E-mail addresses: schauble@ess.ucla.edu, schauble@ucla.edu (E.A. Schauble).

0016-7037/$ - see front matter © 2006 Elsevier Inc. All rights reserved.
doi:10.1016/j.gca.2006.02.011

For more than 50 years, the abundances of the stable isotopes of oxygen in carbonate minerals have been used to infer ancient variations in water temperatures and polar ice volumes (e.g., Epstein et al., 1953). The oxygen isotope proxy for temperature depends on the temperature sensitivity of the isotope exchange reaction:

$$H_2{}^{18}O + CaC^{16}O_3 \leftrightarrow H_2{}^{16}O + CaC^{18}O^{16}O_2$$

The equilibrium constant for this reaction decreases with increasing temperature. As a result, the temperature of formation of the carbonate can be determined if (1) an equilibrium isotopic signature is acquired during crystallization and subsequently retained, (2) $^{18}O/^{16}O$ ratios of carbonate minerals can be measured with sufficiently high precision, (3) the equilibrium isotopic fractionation between carbonate and water as a function of temperature is known, and (4) the $^{18}O/^{16}O$ ratio of the water that the carbonate precipitated from is known. This last condition is often not met. For example, during glacial intervals the storage of ^{16}O-rich water in ice caps caused the oceans to have higher $^{18}O/^{16}O$ ratios than the modern ocean, requiring independent constraints on the ocean's $\delta^{18}O$ before ocean temperature can be determined from the H_2O–$CaCO_3$ isotopic exchange equilibrium. Potential applications of O-isotope paleothermometry to Paleozoic and Precambrian climates, non-oceanic environments, and extraterrestrial hydrothermal systems are also hampered by uncertainties in the $^{18}O/^{16}O$ ratios of carbonate-precipitating waters. In such cases it would be helpful to have an independent means to reconstruct temperature. This study examines the theoretical foundation of one such approach—an internal isotopic ordering, or clumping reaction to form $^{13}C^{18}O^{16}O_2{}^{2-}$ in carbonate minerals. Analytical methods for the measurement of $^{13}C^{18}O^{16}O_2{}^{2-}$, along with experimental and empirical calibrations of the $^{13}C^{18}O^{16}O_2{}^{2-}$-forming reaction are discussed in a companion paper (Ghosh et al., 2006).

We are not aware of any previous efforts to measure or theoretically estimate non-stochastic abundances of multiply substituted isotopologues in minerals. However, previous attempts have been made to develop single-mineral thermometers using intra-crystalline oxygen-isotope fractionations (e.g., Hamza and Epstein, 1980; Bechtel and Hoernes, 1990), which in principle could be used in similar ways to determine temperatures of mineral precipitation in systems where the isotopic composition of the fluid phase is not known.

1.1. Multiply substituted carbonate isotopologues

The common carbonate minerals are molecular crystals (Fig. 1), containing separate $CO_3{}^{2-}$ carbonate groups with strong internal C–O bonds bound to the crystal lattice by weaker cation-oxygen (e.g., Ca^{2+}–O) bonds. The isotopic 'clumping' reactions studied here involve the exchange of ^{13}C, ^{18}O, and ^{17}O between carbonate molecules in the crystal lattice, creating a distribution of singly and multiply substituted species (isotopologues):

$$^{12}C^{18}O^{16}O_2{}^{2-} + {}^{13}C^{16}O_3{}^{2-} \leftrightarrow {}^{13}C^{18}O^{16}O_2{}^{2-} + {}^{12}C^{16}O_3{}^{2-} \quad (1)$$

$$^{12}C^{17}O^{16}O_2{}^{2-} + {}^{12}C^{18}O^{16}O_2{}^{2-} \leftrightarrow {}^{12}C^{18}O^{17}\,O^{16}O^{2-} + {}^{12}C^{16}\,O_3{}^{2-} \quad (2)$$

Reactions (1) and (2) differ from the H_2O–CO_2 oxygen isotope exchange reaction in that all of the exchange components are present in one mineral phase, making the equilibrium constant an internal property that is not affected by the isotopic compositions of other phases in the system. Most importantly, the equilibrium constants for these internal isotopic exchange reactions should be nearly independent of the isotopic composition of coexisting water and of the bulk $^{18}O/^{16}O$, $^{17}O/^{16}O$, and $^{13}C/^{12}C$ ratios of the crystal. There is not strict independence because weak interactions between separated $CO_3{}^{2-}$ molecules in the carbonate crystal give rise to non-idealities in the activity–composition relationships for the various carbonate-ion isotopologues. However, we estimate that these effects are insignificant for present purposes (see the Section 3, below).

We focus on reactions (1) and (2) because the multiply substituted isotopologues $^{13}C^{18}O^{16}O_2{}^{2-}$ and $^{12}C^{18}O^{17}O^{16}O^{2-}$ contribute ~96% and 3%, respectively, of the mass-47 signal in CO_2 generated by phosphoric-acid digestion. This estimate assumes initial $\delta^{18}O_{VSMOW} \approx 0$ and $\delta^{13}C_{VPDB} \approx 0$ in the carbonate, and that one C–O bond in each $CO_3{}^{2-}$ group is broken at random during the acid reaction. Other multiply substituted carbonate isotopologues are much less abundant, contributing less than 1% to the measured mass-47 CO_2 signal, and are ignored for this initial study.

1.2. Thermodynamics of multiply substituted isotopologues

The thermodynamic energy governing the relative abundances of singly and multiply substituted isotopologues of carbonate, CO_2, and other molecules is closely related to the driving energy for intermolecular and inter-crystalline stable-isotope fractionation, arising from small differences in the vibrational energies of isotopically substituted molecules (e.g., Urey, 1947). $CO_3{}^{2-}$ molecules that have been substituted with one heavy isotope (^{13}C, ^{17}O or ^{18}O) vibrate at lower frequencies than molecules containing only the more common light isotopes. This reduces the zero-point vibrational energy ($=1/2\sum h\nu$ for harmonic oscillators) of the isotopically heavy molecule, stabilizing it relative to the isotopically light form. Similarly, a carbonate molecule with multiple heavy-isotope substitutions (e.g., $^{13}C^{18}O^{16}O_2{}^{2-}$) vibrates at still lower frequencies, and has a correspondingly smaller zero-point energy. In general, substituting a heavy isotope into a molecule that already contains another heavy isotope has a larger effect on the frequencies and zero-point energy than an equivalent

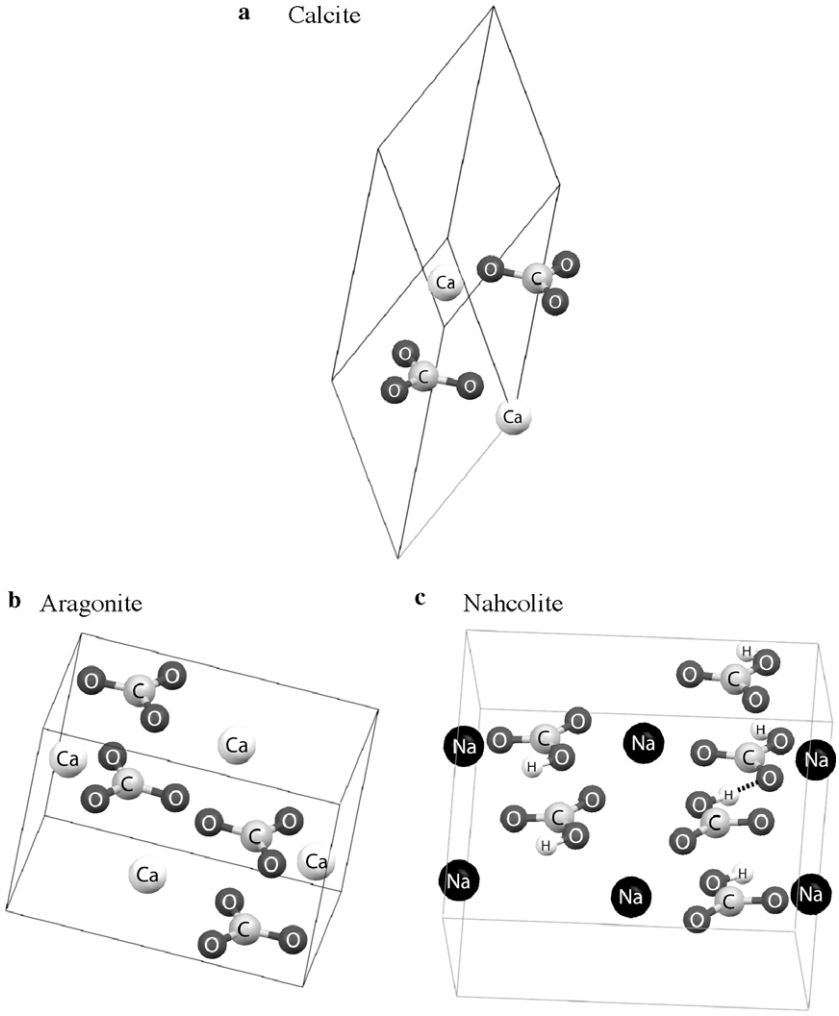

Fig. 1. Crystal structures of carbonates: (a) calcite; (b) aragonite; and (c) nahcolite. In order to show complete CO_3^{2-} and HCO_3^- groups and hydrogen-bonding relationships the images of calcite and nahcolite show some atoms beyond the boundary of the depicted unit cell. The dashed line shows one of the hydrogen bonds in nahcolite.

substitution into an isotopically light molecule would—i.e., there is a small non-linearity in progressive heavy-isotope substitutions (Wang et al., 2004).

For example, in CO_2 the isotopic exchange reaction:

$$^{12}C^{18}O^{16}O + {}^{13}C\,{}^{16}O_2 \leftrightarrow {}^{13}C^{18}O^{16}O + {}^{12}C^{16}O_2 \quad (3)$$

is driven towards the right because the total zero-point energy of the right-hand side is lower (by ~5 J/mol for CO_2) than the zero-point energy of the left-hand side. At equilibrium, the system will therefore have a greater abundance of $^{13}C^{18}O^{16}O$ and $^{12}C^{16}O_2$ than would be expected if carbon and oxygen isotopes were distributed randomly. At room temperature the K_{eq} for this reaction in CO_2 is approximately 1.0009 (after accounting for translational, rotational, and excited vibrational energies in addition to the zero-point energy) (Eiler and Schauble, 2004; Wang et al., 2004).

For most natural materials the light ^{12}C and ^{16}O isotopes dominate (atomic abundances of ~98.9% and 99.8%, respectively (Parrington et al., 1996)), while ^{17}O is far less abundant (~0.04%) than ^{18}O (~0.20%). This means that $^{12}C^{16}O_2$ and the singly substituted $^{12}C^{18}O^{16}O$ and $^{13}C^{16}O_2$ molecules predominate at molecular masses of 44, 45, and 46, respectively, of natural CO_2, and variations in the internal exchange equilibrium, reaction 3, are reflected mainly as variations in the abundance of the least common component, $^{13}C^{18}O^{16}O$. CO_2 at room-temperature equilibrium thus has a ~1‰ excess of mass-47 isotopologues (Eiler and Schauble, 2004; Wang et al., 2004).

2. Methods

2.1. Modeling the thermodynamics of carbonate isotopologues

Equilibrium constants for reaction (1)—formation of $^{13}C^{18}O^{16}O_2{}^{2-}$—are calculated for calcite, aragonite, dolomite, magnesite, witherite, and nahcolite. These were chosen to include the most common carbonate minerals

as well as a wide variety of structures and crystal-chemical environments. The equilibrium constant for reaction (2)—the formation of $^{12}C^{18}O^{17}O^{16}O^{2-}$—is estimated in calcite only. The driving energies for each reaction are estimated from the vibrational (phonon) Helmholtz free energies of isotopically substituted crystals. All calculations assume that vibrations are harmonic, and that the electronic structures are not affected by atomic masses (Born–Oppenheimer approximation).

Although high quality Raman and infrared phonon frequency measurements have been published for zero wave-vector modes in calcite, aragonite, dolomite, and magnesite (e.g., Porto, 1966; Hellwege et al., 1970; Rutt and Nicola, 1974; Frech et al., 1980) these data are not sufficient to accurately quantify vibrational free energies, so it is necessary to create vibrational models for each mineral. Spectroscopic selection rules for these structures indicate that some zero wave-vector modes are neither infrared active nor Raman active. In addition infrared and Raman measurements are only sensitive to phonons with zero wave vector, while the phonon density of states controlling thermodynamic properties is dominated by non-zero wave-vector phonons. An inelastic neutron scattering study of phonons from several non-zero wave vectors in calcite (Cowley and Pant, 1973) concentrated on low-frequency modes, which do not contribute as strongly to C- and O-isotope partitioning as do high-frequency modes (Chacko et al., 1991). Furthermore, very little is known about phonon frequencies in isotopically substituted carbonates (e.g., Gillet et al., 1996), and even less is known about crystals with multiply substituted isotopologues. For all of these crystals it is thus necessary to construct force-field models to estimate unknown vibrational frequencies. We used first-principles electronic structure calculations, in the form of density functional perturbation theory (DFPT), to create vibrational models for each carbonate mineral studied.

For each mineral structure we approximate the Helmholtz free energy with a simplified model of the vibrational density of states. The Helmholtz free energy of pure ^{12}C–^{16}O crystals is estimated by calculating a finite number (30–150) of phonon frequencies for each mineral at 1–5 phonon wave vectors (i.e., q in the standard wave equation $f(x,t) = A \cdot \sin(qx - \omega t)$, where A is amplitude, x is the position vector, $\omega/2\pi$ is the oscillation frequency and t is time). Phonon wave vectors are chosen to take advantage of unit cell symmetry, forming a shifted Monkhorst–Pack-like grid sampling the Brilluoin zone of each mineral (Gonze et al., 2002). The Helmholtz free energies of isotopically substituted crystals are approximated by calculating frequencies for the same phonons in model crystals with one $^{12}C^{16}O_3^{2-}$ group per unit cell replaced by $^{13}C^{16}O_3^{2-}$, $^{12}C^{18}O^{16}O_2^{2-}$, or $^{13}C^{18}O^{16}O_2^{2-}$. The goal is to sample enough phonons for each mineral and isotopologue to achieve a converged estimate of the reduced partition function:

$$Q_{\mathrm{red}} = \left(\prod_{i=1}^{3N_{\mathrm{atom}}N^*_{\mathrm{qpt}}} \nu_i \frac{\exp\frac{-h\nu_i}{2k_{\mathrm{B}}T}}{1-\exp\frac{-h\nu_i}{k_{\mathrm{B}}T}} \right)^{1/N^*_{\mathrm{qpt}}}$$

where N_{atom} is the total number of atoms per unit cell, N^*_{qpt} is the number of phonon wave vectors sampled—including all symmetric images within the upper half of the Brillouin zone, ν_i are the phonon frequencies, T is the absolute temperature, h is Planck's constant (6.62607×10^{-34} J s, and k_{B} is Boltzmann's constant (1.38065×10^{-23} J/K). The reduced partition functions are then used to calculate equilibrium constants using the standard relation:

$$K_{\mathrm{eq}}[3866] = \frac{Q_{\mathrm{red}}(\mathrm{M}^{13}\mathrm{C}^{18}\mathrm{O}^{16}\mathrm{O}_2) \times Q_{\mathrm{red}}(\mathrm{M}^{12}\mathrm{C}^{16}\mathrm{O}_3)}{Q_{\mathrm{red}}(\mathrm{M}^{12}\mathrm{C}^{18}\mathrm{O}^{16}\mathrm{O}_2) \times Q_{\mathrm{red}}(\mathrm{M}^{13}\mathrm{C}^{16}\mathrm{O}_3)}.$$

Here, $K_{\mathrm{eq}}[3866]$ is a shorthand notation indicating the doubly substituted species, $^{13}C^{18}O^{16}O_2^{2-}$, formed on the right-hand side of reaction (1). Note that the symmetry number ratio for this reaction cancels to unity, so we have omitted symmetry terms from the expression. We also calculated the equilibrium constant for reaction (2) in calcite using the same techniques. The symmetry number ratio for reaction (2) is 2/3 rather than unity. Relative to a stochastic distribution, excess $^{12}C^{18}O^{17}O^{16}O^{2-}$ is indicated by $K_{\mathrm{eq}}[2876] > 2/3$.

In aragonite and witherite (an aragonite-like structure) there are two crystallographically distinct oxygen sites (O1 and O2), leading to two possible sites of ^{18}O substitution, and nahcolite has three distinct oxygen sites. We have made separate models accounting for substitution at each crystallographically distinct site to see if preferential formation of ^{13}C–^{18}O bonds is position-dependent. Reduced partition function ratios for $^{13}C/^{12}C$ and $^{18}O/^{16}O$ substitution are calculated in an intermediate step for each crystal and crystallographic site. These reduced partition function ratios can be compared to theoretical and experimental C- and O-isotope fractionation data to evaluate model accuracies.

2.2. Density functional perturbation theory

Phonon frequencies in carbonate crystals are modeled using DFPT, as implemented in the ABINIT software package (Gonze et al., 2002. www.abinit.org). ABINIT simplifies the calculation crystal energies, forces, and higher-order properties by approximating nuclear charges and inner-shell (i.e., non-valence) electrons with a pseudopotential, and the near-nucleus portion of valence electron wave functions with pseudo-wave-functions. Pseudo-wave-functions of valence electrons are built up from a linear combination of plane waves. All calculations reported here used the gradient-corrected density functional of Perdew, Burke, and Ernzerhof, hereafter abbreviated PBE (Perdew et al., 1996). In initial models of anhydrous carbonates we tried the Perdew–Zunger functional, based on the local density approximation (Perdew and Zunger,

1981). These models give similar results to the PBE models described here, but generally do not reproduce measured phonon frequencies as well. Gradient-corrected functionals are also better suited to modeling hydrogen-bonded minerals like nahcolite (e.g., Lee et al., 1992). Models of anhydrous carbonates used publicly available Troullier–Martins pseudopotentials for C and O (www.abinit.org). We developed new Rappe–Rabe–Kaxiras–Joannopoulos-type (RRKJ) pseudopotentials (Rappe et al., 1990) for Na, Mg, Ca, and Ba using the OPIUM pseudopotential generator (opium.sourceforge.net). Each pseudopotential was tested for agreement with all-electron atomic calculations over a limited range of ionic configurations, and the absence of spurious bound electronic states (i.e., "ghosts") was confirmed using the method of Gonze et al. (1991). We used the same approach to develop pseudopotentials for O and H for studying nahcolite, because public O and H pseudopotentials for ABINIT were not yet suitable for accurate modeling of hydrous materials with reasonable computational effort. Core radii and reference electronic configurations for the new pseudopotentials are listed in Table 1.

For each mineral species, integration of electronic wave functions over the Brillouin zone is approximated by a sum over a finite number of electronic wave vectors (*k*-points). Crystal symmetries are used to reduce the number of distinct wave vector calculations needed. Optimized wave vector grids for each mineral were chosen semi-automatically using ABINIT's grid generator. Dolomite (space group $R\bar{3}$) was modeled with a weighted sum over six symmetrically distinct *k*-points: $(0,0,-\frac{1}{4})$, $(0,\frac{1}{4},\frac{1}{2})$, $(0,\frac{1}{2},-\frac{1}{4})$, $(\frac{1}{4},\frac{1}{4},-\frac{1}{4})$, $(\frac{1}{4},\frac{1}{4},\frac{1}{4})$, and $(\frac{1}{4},\frac{1}{2},\frac{1}{2})$. Together with all of their symmetric images these form a 32 *k*-point grid in the Brillouin zone. The same grid for the higher symmetry ($R\bar{3}c$) calcite and magnesite structures requires only five distinct *k*-points. The larger unit cells of the orthorhombic carbonates (aragonite and witherite) were modeled with two symmetrically distinct *k*-points: $(\frac{1}{6},\frac{1}{4},\frac{1}{4})$ and $(\frac{1}{2},\frac{1}{4},\frac{1}{4})$, forming a 12 *k*-point grid. Nahcolite was modeled using four distinct *k*-points: $(\frac{1}{8},\frac{1}{4},\frac{1}{4})$, $(\frac{1}{8},\frac{1}{4},-\frac{3}{8})$, $(\frac{3}{8},\frac{1}{4},\frac{3}{8})$, and $(-\frac{3}{8},\frac{1}{4},\frac{1}{8})$, forming a 16 *k*-point grid. In each case the grid of *k*-points was chosen to be dense enough that mineral structures and energies were converged within 0.1% and 0.001 Rydberg/atom (0.014 eV/atom), respectively. Each structure was optimized until residual forces acting on every atom were less than 1×10^{-4} Rydberg/bohr (4×10^{-12} N/m) and unit-cell stresses were less than 1×10^{-6} Rydberg/bohr^3 (1.5×10^{7} Pa).

Planewave energy cutoffs were set at 110 Rydberg (1496 eV) for all of the anhydrous carbonates. This cutoff was sufficient to achieve structural and energy convergence within 0.1% and 0.001 Rydberg/atom, even though the nominal design cutoff for the Ca pseudopotential is 154 Rydberg. Calculations for the hydrous nahcolite structure used an energy cutoff of 82 Rydberg, as the new RRKJ-type Na, O, and H pseudopotentials are well converged at this lower energy.

Calculations were performed on a dual-processor Macintosh G5 computer, and on the Pentium-IV based Geochemistry and Astrobiology Simulator cluster at UCLA.

Table 1
Pseudopotentials developed in this study for density functional perturbation theory calculations

Element	Reference electronic configuration	Cutoff radius (a.u.[a])	Optimal cutoff energy (Rydberg)	Non-linear core correction[b]	Local potential
Na	$3s^{0.2}$	1.80	81	Yes	*p*
	$3p^{0.0}$	2.20	81	$r = 1.5$ a.u.	
	$3d^{0.0}$	1.80	81		
Mg	$3s^{2.0}$	1.75	49	Yes	*p*
	$3p^{0.0}$	1.85	49	$r = 1.4$ a.u.	
	$3d^{0.0}$	1.80	49		
Ca	$3s^{2.0}$	1.40	154	No	*s*
	$3p^{6.0}$	1.40	154		
	$3d^{0.0}$	1.40	154		
	$4s^{0.0}$	1.40	154		
Ba	$5s^{2.0}$	1.68	81	No	*s*
	$5p^{6.0}$	1.68	81		
	$6s^{0.0}$	1.68	81		
	$4f^{0.0}$	1.68	81		
	$5d^{0.0}$	1.68	81		
O	$2s^{2.0}$	1.22	81	No	*d*
	$2p^{4.0}$	1.22	81		
	$3d^{0.0}$	1.22	81		
H	$1s^{1.0}$	0.56	81	No	*s*

All are RRKJ-type norm-conserving pseudopotentials created using OPIUM (opium.sourceforge.net).
[a] 1 a.u. $= 5.29177\times10^{-11}$ m.
[b] Non-linear core correction follows method of Louie et al. (1982).

3. Results and discussion

3.1. Crystal structures and phonon frequencies

Crystal structures optimized with density functional theory are compared with experimental structures in Table 2. Model and observed structures are generally in agreement, with model structure unit cell parameters consistently ~1% too large. This over-estimation of the sizes of unit cells is common in density functional theory calculations using PBE and other gradient-corrected functionals (e.g., Filippi et al., 1994). Calculated zero wave-vector vibrational frequencies for isotopically normal crystals are compared with frequencies measured by IR, Raman, and neutron-scattering spectroscopy in Table 3 and Fig. 2. There is an excellent correlation between model and observed vibrational frequencies, although the model results are about 3% too low. We corrected this underestimation by multiplying model frequencies by a scale factor (1.0331 for anhydrous carbonates, 1.0145 for nahcolite), determined from a linear regression of correlated model and experimental frequencies. Details on correlation between model and observed

Table 2
Calculated and measured crystal structures of carbonate minerals

	Exp.	Model	Mismatch
Calcite—$CaCO_3$ $R\bar{3}c$			
Unit cell			
$a = b = c$ (Å)	6.375	6.434	0.9%
$\angle ab$ (°)	46.08	46.07	0.01°
Volume (Å^3)	122.65	126.05	2.8%
Atom positions (fractional)			
x_o	0.5078	0.5065	
Dolomite—$CaMg(CO_3)_2$ $R\bar{3}$			
Unit cell			
$a = b = c$ (Å)	6.014	6.087	1.2%
$\angle ab$ (°)	47.11	46.97	0.14°
Volume (Å^3)	106.74	110.16	3.2%
Atom positions (fractional)			
x_c	0.2431	0.2429	
x_o	0.4922	0.4924	
y_o	0.9601	0.9635	
z_o	0.2797	0.5065	
Magnesite—$MgCO_3$ $R\bar{3}c$			
Unit cell			
$a = b = c$(Å)	5.676	5.749	1.3%
$\angle ab$ (°)	48.19	48.09	0.10°
Volume (Å^3)	93.09	96.45	3.6%
Atom positions (fractional)			
x_o	0.5280	0.5252	
Aragonite—$CaCO_3$ *Pnma*			
Unit cell			
a (Å)	4.961	4.997	0.7%
b (Å)	7.967	8.011	0.6%
c (Å)	5.740	5.806	1.1%
All angles 90°			
Volume (Å^3)	226.91	232.46	2.4%
Atom positions (fractional)			
y_{Ca}	0.4150	0.4150	
z_{Ca}	0.7597	0.7588	
y_C	0.7622	0.7619	
z_C	0.9138	0.9167	
y_{01}	0.9225	0.9219	
z_{01}	0.9038	0.9078	
x_{02}	0.4736	0.4733	
y_{02}	0.6810	0.6804	
z_{02}	0.9138	0.9141	
Witherite—$BaCO_3$ *Pnma*			
Unit cell			
a (Å)	5.313	5.344	0.6%
b (Å)	8.896	8.945	0.6%
c (Å)	6.428	6.564	2.1%
All angles 90°			
Volume (Å^3)	303.81	313.77	3.3%
Atom positions (fractional)			
y_{Ba}	0.4163	0.4163	
z_{Ba}	0.7549	0.7540	
y_C	0.7570	0.7563	
z_C	0.9190	0.9219	
y_{01}	0.9011	0.9008	
z_{01}	0.9122	0.9148	
x_{02}	0.4595	0.4598	
y_{02}	0.6839	0.6838	
z_{02}	0.9210	0.9215	
Nahcolite—$NaHCO_3$ $P2_1/c$			
Unit cell			
a (Å)	3.51	3.560	1.4%
b (Å)	9.71	9.756	0.5%
c (Å)	8.05	8.186	1.7%
$\angle$ac (°)	111.85	113.26	1.41°
Volume (Å^3)	254.65	261.16	2.6%
Atom positions (fractional)			
x_{Na}	0.4285	0.4245	
y_{Na}	0.0044	0.0047	
z_{Na}	0.7145	0.7126	
x_H	0.669	0.6869	
y_H	0.252	0.2412	
z_H	0.143	0.1494	
x_C	0.2123	0.2120	
y_C	0.2384	0.2389	
z_C	0.9233	0.9232	
x_{01}	0.1893	0.1926	
y_{01}	0.3666	0.3678	
z_{01}	0.9286	0.9284	
x_{02}	0.9896	0.9861	
y_{02}	0.1619	0.1635	
z_{02}	0.7954	0.7945	
x_{03}	0.4959	0.4945	
y_{03}	0.1705	0.1715	
z_{03}	0.0592	0.0606	

The top row for each mineral indicates the stoichiometry and space group. Experimental structures for each mineral are taken from published X-ray and neutron-diffraction studies: calcite, Graf (1961); dolomite, Ross and Reeder (1992); magnesite, Ross (1997); aragonite and witherite, de Villiers (1971); nahcolite, Sauss and Scheuerman (1962), Sharma (1965).

frequencies and the method of calculation of scaling factors are in Appendix A. The scale factors are qualitatively consistent with the model overestimation of unit cell size, since longer bonds generally vibrate at lower frequencies. After scaling, the root-mean-square (rms) misfit between measured phonon frequencies and scaled model results is 10 cm^{-1} for the anhydrous carbonates (considered all together), and 19 cm^{-1} for nahcolite.

We also compared zero wave-vector vibrational frequencies in calcite calculated with the new oxygen pseudopotential to frequencies calculated with the public oxygen pseudopotential. The rms difference between frequencies calculated with the two pseudopotentials is only 0.6 cm^{-1}, suggesting that they are interchangeable without significantly affecting calculated vibrational properties. The similarity further suggests that our results are not strongly affected by the details of pseudopotential construction. The scale factor and rms misfits between measured calcite phonon frequencies and models using either oxygen pseudopotential are statistically indistinguishable.

Recently published (Prencipe et al., 2004) ab initio zero-wave vector phonon frequencies in calcite, calculated with the CRYSTAL software package using a slightly different gradient-corrected density functional and atom-centered

Table 3
Comparison of model and measured zero wave-vector phonon frequencies in carbonate minerals

Calcite	Exp. (cm^{-1})	DFPT (cm^{-1})	Dolomite	Exp. (cm^{-1})	DFPT (cm^{-1})	Magnesite	Exp. (cm^{-1})	DFPT (cm^{-1})
A_{1g}	1088	1094.3	A_g	—	231.2	A_{1g}	1084	1103.3
E_g	156	155.5	A_g	335	338.3	E_g	212	208.4
E_g	283	273.0	A_g	—	876.5	E_g	329	324.4
E_g	714	711.4	A_g	1099	1104.4	E_g	739	737.7
E_g	1432	1437.6	E_g	176	176.2	E_g	1445	1452.6
A_{2u} TO	92	115.9	E_g	301	295.8	A_{2u} TO	230	230.3
A_{2u} TO	303	284.1	E_g	724	724.7	A_{2u} TO	362	365.3
A_{2u} TO	872	867.5	E_g	1444	1446.6	A_{2u} TO	876	868.7
A_{2u} LO	136	145.1	A_u TO	146	160.2	A_{2u} LO	281	278.0
A_{2u} LO	387	398.8	A_u TO	314	303.7	A_{2u} LO	459	464.1
A_{2u} LO	890	881.7	A_u TO	361	357.9	A_{2u} LO	911	895.8
E_u TO	102	118.0	A_u TO	879	870.2	E_u TO	225	229.9
E_u TO	223	211.3	A_u TO	—	1104.7	E_u TO	301	298.4
E_u TO	297	275.8	A_u LO	193	201.5	E_u TO	356	353.4
E_u TO	712	711.3	A_u LO	325	323.6	E_u TO	747	745.8
E_u TO	1407	1406.0	A_u LO	429	442.7	E_u TO	1436	1435.8
E_u LO	123	131.2	A_u LO	901	889.9	E_u LO	241	240.5
E_u LO	239	222.8	A_u LO	—	1104.7	E_u LO	315	303.3
E_u LO	380	376.1	E_u TO	150	158.4	E_u LO	475	476.6
E_u LO	715	712.5	E_u TO	255	246.4	E_u LO	763	748.7
E_u LO	1549	1555.9	E_u TO	345	340.5	E_u LO	1599	1600.3
A_{2g}	173	183.6	E_u TO	728	728.1	A_{2g}	—	304.0
A_{2g}	—	310.4	E_u TO	1435	1426.7	A_{2g}	—	361.7
A_{2g}	—	872.5	E_u LO	173	178.8	A_{2g}	—	875.9
A_{1u}	—	284.5	E_u LO	271	259.4	A_{1u}	—	370.0
A_{1u}	—	1093.6	E_u LO	439	441.8	A_{1u}	—	1105.3
			E_u LO	741	730.3			
			E_u LO	1580	1579.5			

Aragonite	Exp. (cm^{-1})	DFPT (cm^{-1})	Witherite	Exp. (cm^{-1})	DFPT (cm^{-1})	Nahcolite	Exp. (cm^{-1})	DFPT (cm^{-1})
A_g	142	144.9	A_g	—	77.8	A_g	—	76.7
A_g	161	156.4	A_g	—	93.4	A_g	—	84.9
A_g	193	184.4	A_g	—	136.9	A_g	—	123.7
A_g	214	189.7	A_g	—	145.5	A_g	—	147.0
A_g	284	274.4	A_g	—	215.2	A_g	—	152.3
A_g	705	702.1	A_g	689	691.0	A_g	—	158.2
A_g	853	857.7	A_g	847	861.4	A_g	—	200.4
A_g	1085	1097.2	A_g	1060	1072.5	A_g	—	209.1
A_g	1462	1464.9	A_g	1420	1420.6	A_g	—	223.8
A_u	—	58.0	A_u	—	74.2	A_g	—	652.6
A_u	—	132.0	A_u	—	132.3	A_g	—	687.6
A_u	—	141.2	A_u	—	167.9	A_g	—	818.9
A_u	—	254.2	A_u	—	192.5	A_g	1047	1031.4
A_u	—	691.7	A_u	—	690.6	A_g	—	1078.6
A_u	—	1396.3	A_u	—	1388.6	A_g	—	1265.4
B_{1g}	112(?)	93.2	B_{1g}	—	77.9	A_g	—	1482.6
B_{1g}	152(?)	149.9	B_{1g}	—	130.3	A_g	—	1623.3
B_{1g}	—	193.5	B_{1g}	—	160.9	A_g	—	2564.5
B_{1g}	—	209.0	B_{1g}	—	185.4	B_g	—	95.4
B_{1g}	721(?)	703.4	B_{1g}	1509(?)	1428.9	B_g	—	108.0
B_{1g}	—	1464.9	B_{1g}	710	693.9	B_g	—	141.9
B_{2g}	180(?)	168.5	B_{2g}	—	91.9	B_g	—	161.7
B_{2g}	206(?)	205.8	B_{2g}	—	133.7	B_g	—	166.6
B_{2g}	248(?)	245.1	B_{2g}	—	151.0	B_g	—	174.0
B_{2g}	—	252.5	B_{2g}	—	181.8	B_g	—	195.6
B_{2g}	266(?)	273.0	B_{2g}	—	222.3	B_g	—	240.2
B_{2g}	717(?)	712.8	B_{2g}	699	698.6	B_g	—	344.8
B_{2g}	907(?)	900.0	B_{2g}	—	882.5	B_g	—	643.7
B_{2g}	—	1093.8	B_{2g}	—	1071.0	B_g	—	689.9
B_{2g}	1574(?)	1585.3	B_{2g}	1450(?)	1517.8	B_g	—	821.8
B_{3g}	123	94.0	B_{3g}	—	85.2	B_g	—	1024.4
B_{3g}	180	156.6	B_{3g}	—	142.5	B_g	—	1064.1
B_{3g}	190	174.6	B_{3g}	—	157.2	B_g	—	1418.0
B_{3g}	272	264.6	B_{3g}	—	208.0	B_g	—	1445.5

Table 3 (*continued*)

Aragonite	Exp. (cm^{-1})	DFPT (cm^{-1})	Witherite	Exp. (cm^{-1})	DFPT (cm^{-1})	Nahcolite	Exp. (cm^{-1})	DFPT (cm^{-1})
B_{3g}	701	698.9	B_{3g}	—	690.3	B_g	—	1712.7
B_{3g}	—	1418.2	B_{3g}	1539(?)	1404.2	B_g	—	2748.6
B_{1u} TO	—	142.6	B_{1u} TO	—	75.5	A_u TO	—	67.9
B_{1u} TO	—	187.4	B_{1u} TO	—	141.1	A_u TO	—	115.9
B_{1u} TO	—	231.9	B_{1u} TO	—	174.5	A_u TO	—	125.4
B_{1u} TO	—	291.0	B_{1u} TO	—	224.9	A_u TO	—	143.9
B_{1u} TO	713	709.4	B_{1u} TO	—	883.1	A_u TO	—	178.2
B_{1u} TO	—	901.0	B_{1u} TO	694	694.0	A_u TO	255	222.8
B_{1u} TO	1085	1095.4	B_{1u} TO	1059	1072.0	A_u TO	255	231.1
B_{1u} TO	1466	1476.2	B_{1u} TO	1449	1427.2	A_u TO	—	334.0
B_{2u} TO	—	52.8	B_{2u} TO	—	130.6	A_u TO	—	641.0
B_{2u} TO	—	153.6	B_{2u} TO	—	153.5	A_u TO	—	690.0
B_{2u} TO	—	187.2	B_{2u} TO	—	162.9	A_u TO	812	821.6
B_{2u} TO	699	697.1	B_{2u} TO	694	692.3	A_u TO	997	1008.0
B_{2u} TO	1443	1447.5	B_{2u} TO	1449	1423.7	A_u TO	—	1062.6
B_{3u} TO	—	171.6	B_{3u} TO	—	134.9	A_u TO	1398	1409.5
B_{3u} TO	—	190.7	B_{3u} TO	—	140.0	A_u TO	—	1448.7
B_{3u} TO	—	262.3	B_{3u} TO	—	156.4	A_u TO	1655	1643.4
B_{3u} TO	—	285.4	B_{3u} TO	—	230.5	A_u TO	2650(?)	2668.9
B_{3u} TO	—	716.3	B_{3u} TO	—	703.5	B_u TO	—	119.1
B_{3u} TO	853	857.0	B_{3u} TO	857	860.7	B_u TO	—	135.7
B_{3u} TO	1083	1094.5	B_{3u} TO	—	1072.1	B_u TO	—	169.2
B_{3u} TO	—	1471.2	B_{3u} TO	—	1415.9	B_u TO	—	174.5
						B_u TO	—	197.5
						B_u TO	255	214.4
						B_u TO	—	254.5
						B_u TO	656	651.8
						B_u TO	694	688.8
						B_u TO	—	818.8
						B_u TO	1032	1031.0
						B_u TO	1045	1078.6
						B_u TO	1300	1269.9
						B_u TO	1452	1470.0
						B_u TO	1617	1617.7
						B_u TO	2542	2533.8

Model frequencies reported here have been scaled by 1.0331 for anhydrous carbonates, and by 1.0145 for nahcolite. Some uncertain correlations (indicated by question marks) are not used in calculating scale factors and rms errors.

Experimental data are from published Raman, infrared, and neutron scattering studies: calcite, Cowley and Pant (1973); Hellwege et al. (1970); Porto (1966); dolomite, Nicola et al. (1976); Hellwege et al. (1970); magnesite, Rutt and Nicola (1974); aragonite, Frech et al. (1980); Martens et al. (2004); witherite, Pasierb et al. (2001); Martens et al. (2004); and nahcolite, Bertoluzza et al. (1981). For calcite, aragonite, and dolomite we have followed the tabulation of Pilati et al. (1998) as closely as possible.

basis sets, showed a very similar correlation with experiment (rms error ~14 cm^{-1} after scaling). The scale factor for the CRYSTAL model frequencies is even closer to unity (~0.993) than the DFPT result. Prencipe et al. (2004) also calculated frequency shifts in ^{13}C- and ^{18}O-substituted calcite, which are generally in very good agreement our results.

3.2. Equilibrium constants

Estimated equilibrium constants for reaction (1) (K_{eq}[3866]) are shown in Table 4 and Fig. 3. These results show that carbonate minerals formed at equilibrium will contain $^{13}C^{18}O^{16}O_2^{2-}$ ionic groups in excess of those expected for a stochastic distribution of isotopes throughout carbonate mineral lattices. The magnitude of the excess decreases as temperature increases, and is roughly linear when plotted against $1/T^2$ or $1/T$ (Fig. 3). The excess is approximately 0.5‰ at 273.15 K, 0.4‰ at 298.15 K, and is less than 0.1‰ for temperatures above 575 K. From 273 to 303 K the sensitivity of K_{eq}[3866] to temperature is roughly −0.000003/K (−0.003‰/K). Initial measurements (Ghosh et al., 2006) suggest that measurement to ±0.01‰ accuracy will be possible, indicating that temperature can be constrained to within ±3 K. The equilibrium constants are sparingly sensitive to the details of phonon density-of-states sampling, varying by 3×10^{-5} from the smallest sample (30 phonons) to the largest sample (150 phonons) in calcite and less than 1×10^{-6} between 60- and 120-phonon samples of aragonite. The most accurate estimates are expected to come from the densest sampling, which are indicated in bold type in the table.

3.3. Crystal chemistry of K_{eq}[3866]

Our best-estimate equilibrium constants are very similar for all of the carbonate minerals studied, with a total

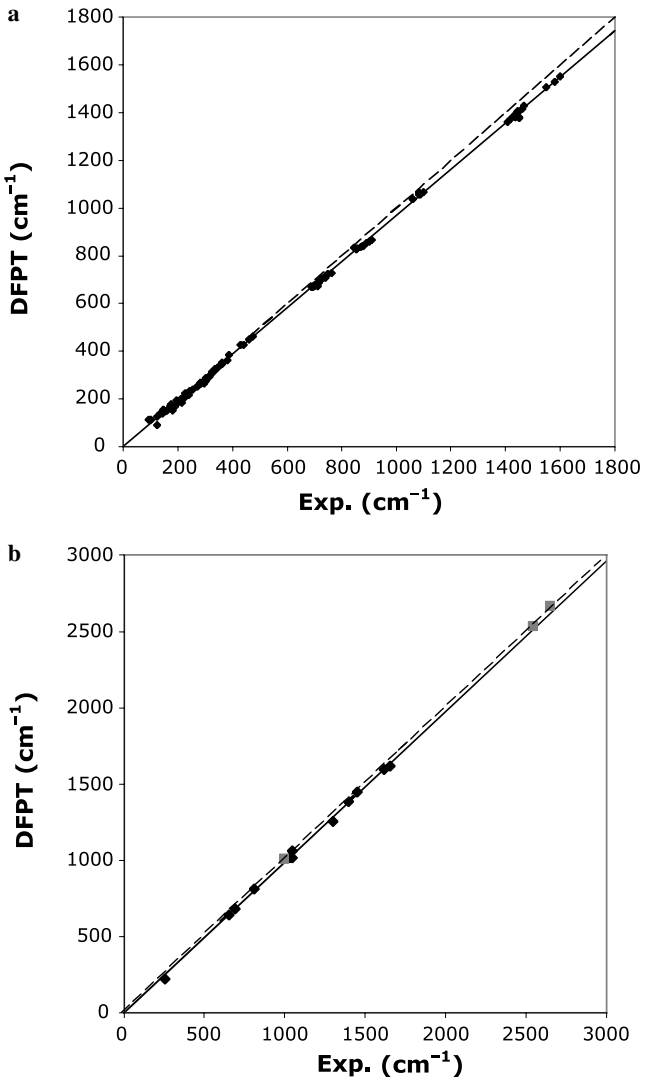

Fig. 2. Comparison of model (DFPT) and measured zero wave-vector phonon frequencies. (a) Anhydrous carbonates: calcite, dolomite, magnesite, aragonite, and witherite. The best-fit line through the origin (solid line) corresponds to a scale factor of ν(measured) = 1.0331 · ν(DFPT). The dashed line indicates 1:1 correlation. (b) Nahcolite. Linear regression ν(measured) ≈ 1.0145 · ν(DFPT) is shown as a solid line. The dashed line indicates 1:1 correlation. Gray symbols indicate O–H stretching and C–O–H bending modes not included in the linear regression.

range of less than 0.03‰ at 298 K, even though we have modeled a wide variety of crystal types. Indeed, equilibrium constants calculated for an isolated CO_3^{2-} group in the gas phase are within this range, if the vibrational frequencies are scaled to match the frequencies of CO_3^{2-} internal vibrations in calcite (W. Guo, pers. communication). This remarkable uniformity suggests that the crystal chemical environment surrounding the carbonate group has a only a weak effect on K_{eq}[3866]. If true, it is likely that other carbonate minerals like siderite ($FeCO_3$), ankerite ($CaFe(CO_3)_2$) and vaterite ($CaCO_3$) will show similar behavior, as will impure and/or non-crystalline phases like aqueous solutions and carbonate apatites. In this sense, it may not be necessary to characterize the precise chemical composition of measured samples, and temperature signals in crystals may be useful even when they are inherited from aqueous HCO_3^- or CO_3^{2-} (rather than being determined by the solid-state homogeneous equilibrium).

Crystallographically distinct oxygen sites exhibit different local values of K_{eq}[3866], especially in nahcolite (Fig. 3c). This variability probably reflects differences in C–O bond order within the HCO_3^- groups, with the protonated C–O–H subgroup (bond order ~1) exhibiting less excess ^{13}C–^{18}O clumping, a strongly hydrogen-bonded C–O bond (bond order <1.5) intermediate and the non-hydrogen bonded C–O (bond order >1.5) having the most pronounced ^{13}C–^{18}O excess. Small differences are also predicted for the two oxygen sites in aragonite and witherite. The correlation between bond order and K_{eq}[3866] observed in carbonates agrees well with equilibrium constants for formation of excess ^{13}C–^{18}O-substituted gas phase molecules (Fig. 4.; Wang et al., 2004). This suggests that equilibria involving multiply substituted isotopologues of other substances could be crudely estimated from their molecular structures alone. For instance, organic ketone ($R_1[C{=}O]R_2$) and aldehyde (R[HC=O]) groups should have a ~1‰ excess of ^{13}C–^{18}O isotopologues at 300 K, like CO_2. C–OH hydroxyl groups in alcohols, with similar C–O bond order as the C–O–H subgroup in nahcolite, would be predicted to have a ~0.3‰ ^{13}C–^{18}O excess at the same temperature.

There are small but systematic differences in equilibrium constant between crystal structures at any one temperature. In the two q-point models, there is a consistent increase in K_{eq}[3866] going from calcite to dolomite to magnesite, as magnesium is progressively substituted for calcium. Aragonite is also predicted to have a slightly higher K_{eq}[3866] than witherite. This pattern suggests an inverse correlation between K_{eq}[3866] and the atomic number of the cation, as is also observed in $^{18}O/^{16}O$ and $^{13}C/^{12}C$ partitioning between carbonates and other phases (e.g. Sheppard and Schwarcz, 1970; Friedman and O'Neil, 1977; Sommer and Rye, 1978; Grossman and Ku, 1986; Chacko et al., 2001). Aragonite is also predicted to have a higher K_{eq}[3866] than calcite, again in the same direction as observed $^{18}O/^{16}O$ and $^{13}C/^{12}C$ fractionations. Nahcolite is so different from the anhydrous carbonates in its crystal chemistry that it is not clear how to interpret the results in this context, especially because its $^{18}O/^{16}O$ and $^{13}C/^{12}C$ fractionation behavior is poorly known. In summary, it appears that K_{eq}[3866], carbon and oxygen isotope fractionations are correlated: carbonates with low-atomic number, "hard" cations and/or the dense aragonite structure tend to have the highest $^{18}O/^{16}O$ and $^{13}C/^{12}C$ and slightly larger $^{13}C^{18}O^{16}O_2^{2-}$ excesses. Of course, crystal-chemical K_{eq}[3866] effects are small and their variations could reflect, at least in part, numerical or model errors.

For each mineral, the temperature dependence of calculated K_{eq}[3866] values can be approximated as a polynomial function of $1/T$. A fourth-order polynomial fit to

Table 4
Equilibrium constants (K_{eq}[3866]) for the reaction: $M^{12}C^{18}O^{16}O_2 + M^{13}C^{16}O_3 \leftrightarrow M^{13}C^{18}O^{16}O_2 + M^{12}C^{16}O_3$ in carbonate minerals, estimated with density functional perturbation theory (DFPT)

Mineral	Number of wave vectors (phonons) sampled	Site	0 °C	25 °C	100 °C	300 °C	1000 °C
Calcite	1 (30)	All C–O bonds equivalent	1.000462	1.000385	1.000229	1.000068	1.000004
$CaCO_3$	2 (60)		1.000482	1.000403	1.000241	1.000073	1.000004
	5 (150)		**1.000490**	**1.000410**	**1.000247**	**1.000075**	**1.000005**
	1 (30)	C, O not in same CO_3^{2-}	0.999999	0.999999	0.999999	1.000000	1.000000
Dolomite	1 (30)	All C–O bonds equivalent	1.000464	1.000388	1.000232	1.000070	1.000004
$CaMg(CO_3)_2$	2 (60)		**1.000484**	**1.000406**	**1.000245**	**1.000075**	**1.000005**
Magnesite	1 (30)	All C–O bonds equivalent	1.000467	1.000391	1.000235	1.000072	1.000005
$MgCO_3$	2 (60)		**1.000498**	**1.000420**	**1.000257**	**1.000081**	**1.000005**
Aragonite	1 (60)	C–O1	1.000542	1.000455	1.000277	1.000086	1.000005
$CaCO_3$	1 (60)	C–O2	1.000496	1.000415	1.000250	1.000076	1.000005
	1 (60)	*Weighted mean*	*1.000511*	*1.000429*	*1.000259*	*1.000079*	*1.000005*
	2 (120)	C–O1	1.000542	1.000456	1.000277	1.000086	1.000006
	2 (120)	C–O2	1.000498	1.000417	1.000251	1.000076	1.000005
	2 (120)	***Weighted mean***	***1.000513***	***1.000430***	***1.000260***	***1.000080***	***1.000005***
Witherite	1 (60)	C–O1	1.000501	1.000418	1.000249	1.000074	1.000005
$BaCO_3$	1 (60)	C–O2	1.000489	1.000408	1.000243	1.000072	1.000004
	1 (60)	***Weighted mean***	***1.000493***	***1.000411***	***1.000245***	***1.000073***	***1.000004***
Nahcolite	1 (72)	C–O–H	1.000320	1.000262	1.000149	1.000040	1.000002
$NaHCO_3$	1 (72)	C–O···H	1.000534	1.000449	1.000273	1.000085	1.000005
	1 (72)	C–O	1.000616	1.000520	1.000320	1.000100	1.000006
	1 (72)	***Mean***	***1.000490***	***1.000410***	***1.000247***	***1.000075***	***1.000004***

Calculated phonon frequencies for calcite, dolomite, magnesite, aragonite and witherite are scaled by 1.0331, to fit measured frequencies; frequencies in nahcolite are scaled by 1.0145. The phonon density of states for each mineral was sampled at one or more symmetrically distinct phonon wave vectors, as indicated. The aragonite and witherite crystal structures each have two distinct oxygen sites, labeled following the convention of de Villiers (1971). Structurally averaged equilibrium constants for these minerals are equal to $K_{eq}(O1)^{1/3} \cdot K_{eq}(O2)^{2/3}$. The three distinct oxygen sites in the nahcolite structure are labeled according to their interaction with hydrogen, with the oxygen site of the C–O–H subunit covalently bonded to carbon and hydrogen, the C–O···H site sharing a strong H-bond with an adjacent HCO_3^- group, and the oxygen site labeled C–O not participating in hydrogen bonding. The average equilibrium constant for nahcolite is determined as $K_{eq}(C–O–H)^{1/3} \cdot K_{eq}(C–O...H)^{1/3} \cdot K_{eq}(C–O)^{1/3}$. Best estimate models for each mineral are indicated in bold type. Italicized entries indicate data averaged over two or more crystallographically distinct sites. Bold type entries indicate best-estimate model result.

~60 points on a uniform $1/T$ grid appears to be sufficient to reproduce each best-estimate $K_{eq}[3866](T)$ to within 3×10^{-6} (0.003‰) from 260 to 1500 K (Table 4). The higher-order expansion is necessary to achieve a good match over a wide range of temperature, due to the substantial curvature at high temperatures (e.g., Fig. 3). A simple linear fit to the 5 q-point calcite $K_{eq}[3866]$ model (in $1/T^2$) from 0 to 50 °C gives the relation: $K_{eq}[3866] = 38.1/T^2 + 0.99998$, as compared with the experimental estimate $K_{eq}[3866] = 59.2/T^2 + 0.99998$ (Ghosh et al., 2006). Accounting for uncertainties in the 0.1–0.2‰ acid-reaction artifact in the experimental results, there is excellent agreement at temperatures >40 °C, but an apparent divergence at lower temperatures. Over the 0–50 °C temperature range experiments suggest that $K_{eq}[3866]$ changes by 0.23‰, while our model indicates a change of only 0.15‰. In the next sections possible sources of error in the theoretical models are discussed.

3.4. Uncertainty in estimated equilibrium constants

The accuracy of the calculated $K_{eq}[3866]$ and $K_{eq}[2876]$ values depends on a number of factors: possible systematic and/or numerical errors in model phonon frequencies of isotopically normal and substituted carbonate minerals, the adequacy of the phonon density of states sampling, anharmonicity, and non-vibrational isotope-dependent energy. We can at least qualitatively evaluate all but the last of these. Phonon density-of-states sampling effects have already been discussed above.

Likely numerical errors appear to cause uncertainties on the order of 1×10^{-5} or less in calculated $K_{eq}[3866]$ and $K_{eq}[2876]$ values, based on three lines of evidence. First, the equilibrium constant calculated for substitution of ^{13}C and ^{18}O in separate CO_3^{2-} groups in the same unit cell of calcite is within 2×10^{-6} of unity (Table 4) at all temperatures above 273 K. Random numerical inaccuracies are expected to displace this equilibrium constant from unity by the same amount as $K_{eq}[3866]$. This result also indicates that adjacent CO_3^{2-} groups interact very weakly, so that a ^{13}C substitution on one group hardly affects (<0.002‰) ^{18}O isotopic substitution in neighboring groups. Second, ABINIT determines phonon frequencies to a numerical precision of 0.001 cm^{-1} (0.0001 cm^{-1} for <1000 cm^{-1} modes), suggesting nominal rounding errors of 0.0005 cm^{-1} or less. This propagates to an uncertainty of

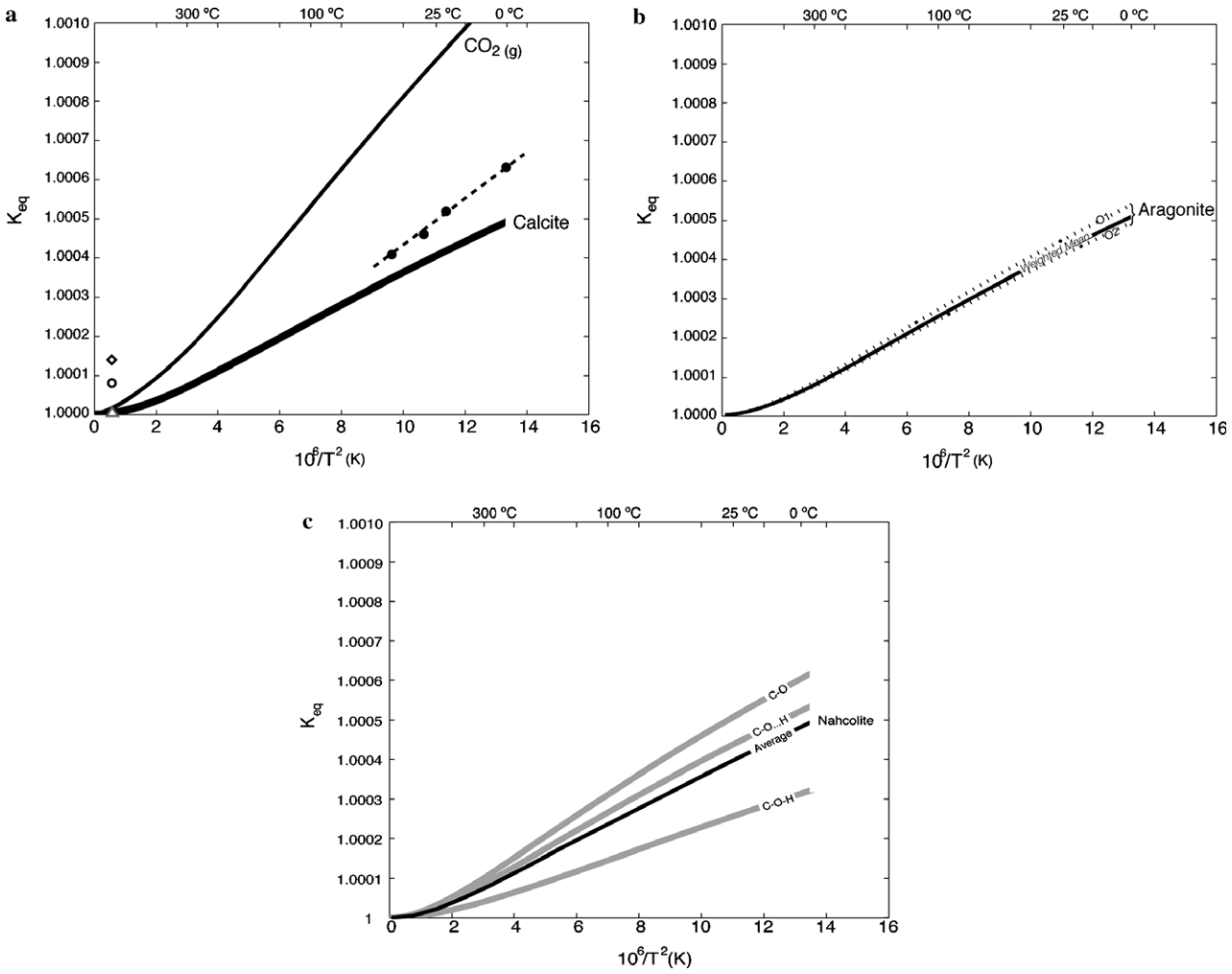

Fig. 3. Equilibrium constants (K_{eq}[3866]) for the reaction: $M^{12}C^{18}O^{16}O_2 + M^{13}C^{16}O_3 \leftrightarrow M^{13}C^{18}O^{16}O_2 + M^{12}C^{16}O_3$ in carbonate minerals. (a) Calcite (5 *q*-point grid). Structurally averaged equilibrium constants for all of the other carbonate minerals are within 0.00003 over the range of temperatures shown. The equilibrium constant for formation of $^{13}C^{18}O^{16}O$ is taken from Wang et al. (2004). Experimental calibration data from Ghosh et al. (2006) are shown for comparison, corrected downwards by 1.4×10^{-4} to account for acid-digestion effects: filled circles are averages from calcites precipated from solution; the open triangle, circle and diamond are ~1100 °C recrystallized Sigma calcite, MZ (Merck) calcite, and New Zealand deep-sea coral 47413, respectively. A linear regression through the synthesis results is indicated with a dashed line. (b) Aragonite. Dotted lines indicate calculated equilibrium constants for the O1 and O2 sites in the structure (de Villiers, 1971). (c) Nahcolite. Gray lines indicate calculated equilibrium constants for the three distinct crystallographic oxygen sites: the C–O–H subgroup, the strongly H– bonded C–O subroup, and the non-H– bonded C–O subgroup (Sauss and Scheuerman, 1962; Sharma, 1965).

roughly 3×10^{-6} to 1×10^{-5} in K_{eq}[3866] at room temperature (the size of the error depends on the number of carbonate groups in each unit cell, increasing roughly as $[N_{CO_3^{2-}}]^{1/2}$). Finally, model phonon frequencies of isotopically substituted crystals generally obey the Redlich–Teller product rule (Angus et al., 1936; Wilson et al., 1955; Chacko et al., 1991) within ~1 part in 10^5, again consistent with average numerical errors of order 0.0001 cm^{-1} for each phonon frequency.

The modest scale factor used to correct systematic underestimation of phonon frequencies in our models should minimize errors in calculated K_{eq}[3866]. However, calculations without this correction are only slightly different from the results reported here. For the five *q*-point model of calcite, K_{eq}[3866] drops from 1.000410 to 1.000383 when the scale factor is omitted, a change of less than 3×10^{-5}, equivalent to ~10 K in an estimated temperature. Reduced partition function ratios for $^{13}C/^{12}C$ and $^{18}O/^{16}O$ exchange are much more sensitive to the frequency scale factor, changing by 5–10‰ if it is omitted. The uncertainty in the slope of the best-fit line used to determine the scale factor for anhydrous carbonates is ~0.1%, suggesting a nominal contribution of 1×10^{-6} to uncertainty in K_{eq}[3866] at 25 °C. In the case of nahcolite, the best-fit slope is much less certain, suggesting a larger nominal error interval of ca. 4×10^{-6} at 25 °C. However, the measured frequencies used in the fitting procedures are themselves uncertain, and correspond to energy differences between the ground state and first excited vibrational state, rather than the energy of the ground state itself, so a realistic

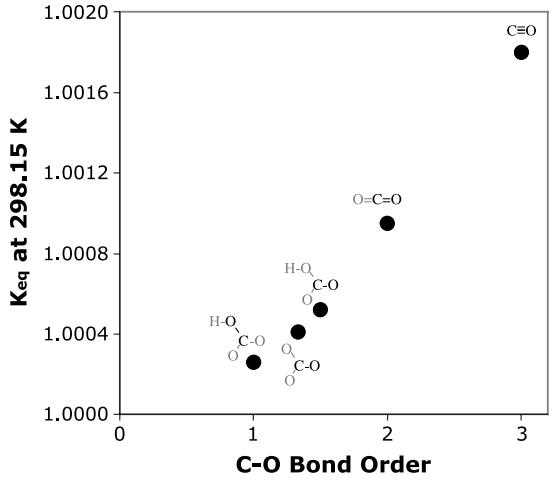

Fig. 4. Variation of the equilibrium constant for formation of ^{13}C–^{18}O bonds with C–O bond order (b.o.). Bold type indicates the relevant bond in each molecule. Data for carbon monoxide (b.o. = 3) and carbon dioxide (b.o. = 2) are taken from Wang et al. (2004). Equilibrium constants for the C–O–H (b.o. = 1) and (non-hydrogen bonded) C–O (b.o. ≈ 1.5) bonds in HCO_3^- are from the present model of nahcolite, and the datum for C–O in anhydrous carbonate (b.o. = 4/3) is from the best-estimate model of calcite.

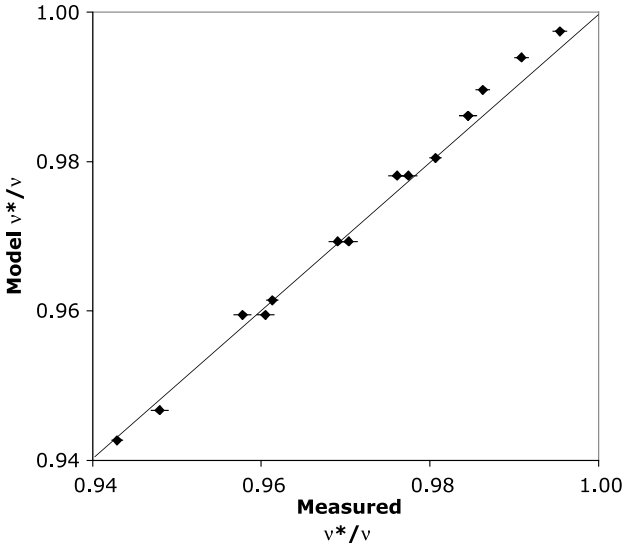

Fig. 5. Comparison of measured and model phonon frequency shifts in ^{18}O-substituted calcite. Each plotted point represents the ratio of a frequency in $^{12}C^{18}O^{16}O_2^{2-}$, $^{12}C^{18}O_2^{16}O^{2-}$, or $^{12}C^{18}O_3^{2-}$ to the frequency of the same mode in $^{12}C^{16}O_3^{2-}$ or unsubstituted (i.e., $^{12}C^{16}O_3^{2-}$ dominated) calcite. Measured ratios are from Raman and infrared spectroscopy data of Gillet et al. (1996). The three points at the extreme upper-right corner are ratios for the ~876 cm^{-1} ν_2 mode. For the ν_4 vibration, both Raman and infrared results are plotted. Slight differences in the measured shifts for this mode yield the three horizontal pairs. Error bars on measured ratios assume a rounding error up to ±0.5 cm^{-1} on each reported frequency. Actual measurement errors may be somewhat larger for some modes.

uncertainty is probably somewhat larger. Measurement uncertainties are probably more or less random, and should not significantly affect estimated scale factors. The latter effect, however, is a consequence of anharmonicity, and is not rigorously quantifiable with available data. The misfit between scaled model frequencies and observations (19 cm^{-1} for nahcolite, ~10 cm^{-1} for the other minerals) is likely to have a modest effect on calculated equilibrium constants. We cannot fully quantify this source of error, but numerical tests on calcite with slightly perturbed model frequencies (preserving model frequency shifts for isotopically substituted lattices) suggests that the 10 cm^{-1} rms misfit propagates to $\sim 1 \times 10^{-5}$ uncertainty in K_{eq}[3866] at 25 °C.

The largest source of uncertainty in our calculations probably comes from systematic errors in calculated frequency differences between isotopically substituted forms of each carbonate mineral. In the present study, we are estimating frequencies for progressive isotopic substitutions, and it is expected that errors of this type will partially cancel each other out. For instance, if a frequency shift is over-estimated in $^{12}C^{18}O^{16}O_2^{2-}$-bearing calcite this indicates that the model normal mode involves too-vigorous motion of the substituted O-atom at the expense of other atoms. Such a model will therefore probably underestimate the shift in $^{13}C^{16}O_3^{2-}$-bearing calcite. The total difference in zero-point energy driving formation of one excess $^{13}C^{18}O^{16}O_2^{2-}$ group is equivalent to a frequency shift of approximately 0.3 cm^{-1}, however, so even modest errors in calculated frequency shifts could bias the estimated equilibrium constant. Gillet et al. (1996) measured infrared and Raman spectra of ^{18}O-enriched synthetic calcite, identifying vibrational frequencies of partially and completely ^{18}O-substituted carbonate molecules within the crystal lattice. These results are compared with the calcite model used in the present study in Fig. 5, showing a strong overall correlation between calculated and observed frequency shifts in $^{12}C^{16}O_3^{2-}$ and $^{12}C^{18}O^{16}O_2^{2-}$, $^{12}C^{18}O_2^{16}O^{2-}$, or $^{12}C^{18}O_3^{2-}$. The largest discrepancies are observed for the ~876 cm^{-1} ν_2 internal vibration, where the DFPT model predicts somewhat smaller frequency shifts than are measured. The difference is consistent through progressive ^{18}O-substitutions, suggesting that measurement error is not the primary cause. The shifts observed by Gillet et al. (1996) in the first overtone to this band (not plotted) in the 1750 cm^{-1} region, where measurement error should be less important, are somewhat closer to the model results. Even considering the overtone data, however, it appears likely that there is a real, if small, inaccuracy in the model. It is not clear how to directly propagate such an error into an uncertainty in the calculated K_{eq}[3866], so we will look at the accuracy of other predicted isotopic properties in the following section.

3.5. $^{13}C/^{12}C$ and $^{18}O/^{16}O$ fractionation

In this section, we test the accuracy of our models by comparing calculated $^{13}C/^{12}C$ and $^{18}O/^{16}O$ fractionation factors with other models and observations. Zero-point energy differences are the primary thermodynamic drivers

of equilibrium O- and C-isotope fractionation factors, so we expect that vibrational models that accurately reproduce these also provide reasonably precise estimates of equilibrium constants for formation of $^{13}C^{18}O^{16}O_2^{2-}$. This is one way to get around the difficulty of estimating model uncertainties arising from the modest disagreement with spectroscopic data in the effect of ^{18}O-substitution on zero wave-vector frequencies in the $\sim$876 cm^{-1} mode of calcite (Gillet et al., 1996). Despite this disagreement, it appears that reduced partition function ratios for $^{18}O/^{16}O$ and $^{13}C/^{12}C$ exchange, calculated with the same phonon frequency models used to estimate K_{eq}[3866], are in good agreement with previous results. If we assume that errors in estimates of K_{eq}[3866] scale in proportion to errors in reduced partition function ratios for $^{13}C/^{12}C$ and $^{18}O/^{16}O$ exchange, a model that reproduces known C- and O-isotope reduced partition function ratios within 1–2‰ out of a total partition function ratio of $\sim$1.1 ($^{18}O/^{16}O$) or 1.2 ($^{13}C/^{12}C$) will have an uncertainty interval of ca. 1×10^{-5} (e.g., $\pm$0.01‰ or $\pm$3 °C) for K_{eq}[3866] values of $\sim$1.0005. This relationship between uncertainties in reduced partition function ratios and K_{eq}[3866] is speculative, but does roughly match the variations observed when the frequency scale factor is omitted (Section 3.4, above).

Here, we compare model $^{13}C/^{12}C$ and $^{8}O/^{16}O$ fractionations in terms of reduced partition function ratios. α_{MCO_3-C} is the ratio $(^{13}C/^{12}C)_{MCO_3}/(^{13}C/^{12}C)_C$, where "C" refers to a monoatomic carbon gas, and α_{MCO_3-O} is the ratio $(^{18}O/^{16}O)_{MCO_3}/(^{18}O/^{16}O)_O$, where "O" refers to a monoatomic oxygen gas. Chacko et al. (1991) estimated reduced partition function ratios for calcite at temperatures from 273 to 4000 K with a simplified, semi-empirical phonon density of states (e.g., Kieffer, 1982). For $^{18}O/^{16}O$, they estimate $\alpha_{Calcite-O} = 1.1203$ and 1.1041 at 273 and 298 K, respectively. Our best model estimates are 1.1196 and 1.1034 at these temperatures, within $\sim$0.6‰ of the Chacko et al. (1991) model. Other lattice-dynamics estimates of $\alpha_{Calcite-O}$ are also in reasonable agreement with our results (Kieffer, 1982; Gillet et al., 1996), with a somewhat larger scatter of up to 1.6‰ at 300 K. For $^{13}C/^{12}C$, Chacko et al. (1991) estimate $\alpha_{Calcite-C} = 1.2339$ and 1.2037 at 273 and 298 K, within 0.7‰ of the present model estimates of 1.2348 and 1.2045. The results of Deines (2004) are somewhat different however, with $\alpha_{Calcite-C} = 1.2264$ and 1.1973 at 273 and 298 K, a disagreement of nearly 7‰. The main difference between the Chacko et al. (1991) and Deines (2004) models is a 27 cm^{-1} discrepancy the frequency of ν_3, the asymmetric C–O stretching mode. However, the present DFPT model is much closer to the Chacko et al. (1991) result despite a calculated ν_3, frequency very close to what Deines (2004) used (1437.6 cm^{-1} vs. 1433 cm^{-1}). The DFPT and Chacko et al. (1991) models match CO_2–$CaCO_3$ fractionation experiments much more closely than the Deines (2004) result. The present model estimates CO_2–$CaCO_3$ fractionations at 30–50 °C that are within 2‰ of those measured by Emrich et al. (1970), for instance.

Calibrations of the calcite–water paleothermometer can also be compared to our model results, if we assume a partition function ratio for liquid water. A recent modeling and experimental study of the reduced partition function of H_2O (Rosenbaum, 1997), combined with calcite synthesis experiments (Kim and O'Neil, 1997) imply $\alpha_{Calcite-O} = 1.1036$ at 25 °C. The model result of 1.1033 is within 0.3‰. Kim and O'Neil measured witherite–water fractionations as well, and along with the Rosenbaum (1997) results these suggest $\alpha_{Witherite-O} = 1.1009$ at 25 °C, about 2.3‰ higher than our model result. In fact, our witherite model appears to consistently underestimate $^{18}O/^{16}O$ partitioning by 2–3‰ from 0 to 300 °C.

A number of studies have investigated inter-mineral oxygen and carbon isotope fractionations between calcite and aragonite or dolomite (e.g., Rubinson and Clayton, 1969; Tarutani et al., 1969; Romanek et al., 1992; and Matthews and Katz, 1977). Model predictions of equilibrium carbonate–carbonate $^{18}O/^{16}O$ and $^{13}C/^{12}C$ fractionations are in good agreement with these experimental results, within 1‰ for calcite, aragonite, and dolomite. However, these inter-mineral fractionations are rather small to begin with (<3‰), and it is not clear how they scale relative to errors in K_{eq}[3866]. The general agreement is therefore only a qualitative confirmation of the model result. It is generally accepted that aragonite preferentially incorporates ^{13}C in low-temperature equilibrium with calcite, with $\Delta^{13}C_{Aragonite-Calcite} \approx 1.8‰$ at 25 °C (Rubinson and Clayton, 1969; Romanek et al., 1992). Our models are in excellent agreement, implying $\Delta^{13}C_{Aragonite-Calcite} = 2.0‰$. Experimental studies have also suggested that aragonite will also have slightly higher $^{18}O/^{16}O$ than coexisting calcite, by $\sim$0.6‰ at 25 °C (Tarutani et al., 1969; Patterson et al., 1993). These results assume an acid fractionation factor of 1.01025 for both aragonite and calcite, but more recent measurements (Kim and O'Neil, 1997) suggest a slightly larger acid fractionation factor for aragonite than calcite (1.01107 vs. 1.01049). Correcting the earlier results, the aragonite–calcite fractionation shrinks to $\sim$0.0‰. Our models actually suggest that aragonite will have slightly lower $^{18}O/^{16}O$ than calcite, by $\sim$0.1‰. The disagreement with experiment is either 0.7‰ or 0.1‰, depending on the acid fractionation factor used. $^{13}C/^{12}C$ fractionation between dolomite and calcite is measured to be $\sim$1.5‰ and 0.7‰ at 100 and 300 °C, respectively (Sheppard and Schwarcz, 1970), compared with model estimates of 1.8‰ and 1.0‰, respectively. Measured dolomite–calcite $^{18}O/^{16}O$ fractionation of 0.7‰ at 300 °C (Matthews and Katz, 1977) is in excellent agreement with a model fractionation of 0.7‰. Earlier measurements of this fractionation (Northrop and Clayton, 1966; Sheppard and Schwarcz, 1970) are also in reasonable agreement (within 0.8‰) with our model results. It should be noted, however, that model O- and C-isotope fractionation factors in dolomite and magnesite may not be fully

converged with respect to phonon wave-vector sampling. Comparing the one-, two- and five q-point models of the rhombohedral carbonates suggests that α_{MCO_3-C} and α_{MCO_3-O} estimates for magnesite and dolomite may be as much as 1‰ too low at 25 °C.

Comparison with experimental and measured O- and C-isotope fractionations suggests that the calcite, aragonite, and dolomite models are consistently accurate within ~1–2‰, while the witherite (and possibly also magnesite and nahcolite) models are somewhat more divergent from experiments and previous theoretical calculations. It is not clear how this level of accuracy will scale with respect to uncertainty in K_{eq}[3866]. If we assume a proportionate scaling, then 1–2‰ errors in O- and C-isotope reduced partition function ratios are suggestive of errors of $\sim 1 \times 10^{-5}$ in K_{eq}[3866]. The relationship between these uncertainties is far from proven, however, and actual errors in K_{eq}[3866] could certainly be larger. Progressive sampling of the phonon density of states in calcite and aragonite suggests a likely convergence error of $\sim 1 \times 10^{-5}$ in K_{eq}[3866]. Possible effects of anharmonicity are much more difficult to quantify. Spectroscopic studies of phonon behavior at high pressures and temperatures, overtone frequencies, and frequency shifts in synthetic, isotopically substituted carbonates suggest that the internal CO_3^{2-} modes are less anharmonic than the lower-frequency external modes (Gillet et al., 1993, 1996). Isotopic fractionation and formation of $^{13}C^{18}O^{16}O_2^{2-}$ seem to be most strongly dependent on the internal modes, suggesting that anharmonic effects are likely to be small. Gillet et al. (1996) estimated an ~1.4‰ effect on α_{MCO_3-O} at room temperature for pressures up to 3 GPa. It is not clear how this error will scale to our calculation of K_{eq}[3866], but a proportionate error would also scale to an effect of order 1×10^{-5}. Errors arising from limited numerical precision, incomplete phonon density of states sampling, imperfect modeling of isotope effects on phonon frequencies (as estimated by consistency with measured $^{13}C/^{12}C$ and $^{18}O/^{16}O$ fractionations), and neglect of anharmonicity therefore suggest an uncertainty of at least 2×10^{-5} to 3×10^{-5} in calculated equilibrium constants. This is necessarily a crude and incomplete error estimate. The apparent discrepancy ($\sim 8 \times 10^{-5}$) between the model results and experiments (Ghosh et al., 2006), is of the same order of magnitude as the estimated uncertainty in the calculated K_{eq}[3866]. However, the sources of error evaluated above are not expected to strongly affect the T-sensitivity of the equilibrium constant, so the observed discrepancy between observations and our theoretical estimate over the 0–50 °C interval is not fully understood.

3.6. Effects of M^{2+}-cation mass on $^{13}C/^{12}C$ and $^{18}O/^{16}O$ fractionation

This study focuses on the tendency of ^{13}C and ^{18}O to form bonds together in carbonate minerals, and we have also found that ^{17}O and ^{18}O preferentially group within the same carbonate molecule in the mineral structures studied, albeit to a lesser extent. These results are consistent with the findings of Wang et al. (2004), indicating a general "heavy likes heavy" rule for isotopic ordering in covalently bonded materials ($^{15}N_2O$ is an exception, because of the strong $^{15}N/^{14}N$ fractionation between the central and distal N-sites). It is interesting to ask whether there is similar behavior in more ionic bonding environments involving heavier elements, like the M^{2+}–O bonds in carbonates. "Heavy likes heavy" in this circumstance would suggest that heavy-element carbonates (like witherite) would have *higher* $^{13}C/^{12}C$ and $^{18}O/^{16}O$ than light-element carbonates like magnesite and calcite, all else being equal. However, experimental calibrations suggest exactly the opposite relationship (e.g., Sheppard and Schwarcz, 1970; Friedman and O'Neil, 1977; Kim and O'Neil, 1997), with heavy-element carbonates tending to be isotopically light. Other properties like ionic radius are also thought to make important contributions to isotopic fractionation in carbonates (e.g., Chacko et al., 2001), and it is not clear which factor is most important (Golyshev et al., 1981; Kim and O'Neil, 1997; Deines, 2004). To examine the effect of cation mass on C- and O-isotope fractionation we have created first-principles lattice–dynamical models of two hypothetical isotopic carbonates: $^{40}MgCO_3$—magnesite (sampling two q-points) and $^{40}BaCO_3$—witherite (one q-point). These models use the same sets of force-constants as the models reported in Tables 4–9, with only the cation masses changed, because force constants are insensitive to isotopic substitution. If cation mass is an important factor controlling equilibrium C- and O-isotope fractionation, we expect these two models to show fractionation factors similar to calcite and aragonite, respectively, since the cation masses are the same. Model results at 25 °C, however, show that fractionation factors for $^{40}MgCO_3$—magnesite are within 0.1‰ of isotopically normal magnesite, and for $^{40}BaCO_3$—witherite they are within 0.05‰ of normal witherite (Table 10), and none resemble calcite and aragonite. Within each mineral type, α_{MCO_3-O} and α_{MCO_3-C} are positively correlated with the mass of the cation: $^{40}BaCO_3$—witherite will have slightly lower $^{13}C/^{12}C$ and $^{18}O/^{16}O$ than normal $^{\sim 137.3}Ba$—witherite, and normal $^{\sim 24.3}MgCO_3$—magnesite will also have lower $^{13}C/^{12}C$ and $^{18}O/^{16}O$ than $^{40}MgCO_3$—magnesite. These results indicate that the

Table 5
Equilibrium constants (K_{eq}[2876]) for the reaction: $Ca^{12}C^{18}O^{16}O_2 + Ca^{12}C^{17}O^{16}O_2 \leftrightarrow Ca^{12}C^{18}O^{17}O^{16}O + Ca^{12}C^{16}O_3$ in calcite

Mineral	Number of wave vectors (phonons) sampled	Site	0 °C	25 °C	100 °C	300 °C	1000 °C
Calcite	1 (30)	All C–O bonds equivalent	0.666733	0.666719	0.666693	0.666673	0.666667
	2 (60)		0.666729	0.666715	0.666691	0.666672	0.666667

The high-temperature (stochastic) equilibrium constant is 2/3. Scale factors and density-of-states sampling are the same as for K_{eq}[3866].

Table 6
Polynomial fits to calculated best-estimate equilibrium constants

Mineral	A	B	C	D
Calcite [$CaCO_3$]	-3.40752×10^{6}	2.36545×10^{4}	-2.63167	-5.85372×10^{-3}
Dolomite [$MgCa(CO_3)_2$]	-3.39320×10^{6}	2.33452×10^{4}	-2.08619	-6.03563×10^{-3}
Magnesite [$MgCO_3$]	-3.39358×10^{6}	2.23628×10^{4}	3.29116	-8.79426×10^{-3}
Aragonite [$CaCO_3$]	-3.51109×10^{6}	2.40017×10^{4}	-4.62181×10^{-1}	-7.25553×10^{-3}
Witherite [$BaCO_3$]	-3.44192×10^{6}	2.44332×10^{4}	-5.10813	-4.75518×10^{-3}
Nahcolite [$NaHCO_3$]	-3.32412×10^{6}	2.28043×10^{4}	-8.18379×10^{-2}	-7.97428×10^{-3}

Each fit has the form: $K_{eq}[3866](T) = A/T^4 + B/T^3 + C/T^2 + D/T + 1$. These reproduce equilibrium constants within 3×10^{-6} (0.003‰) from 260 to 1500 K.

Table 7
Polynomial fit to calculated best-estimate equilibrium constants $K_{eq}[2876]$ for formation of $Ca^{12}C^{18}O^{17}O^{16}O$

Mineral	A	B	C	D
Calcite	-2.81387×10^{5}	3.26769×10^{3}	-3.98299	1.68454×10^{-3}

In this fit, $K_{eq}(T) = A/T^4 + B/T^3 + C/T^2 + D/T + 2/3$. The calculated equilibrium constant is reproduced within 2×10^{-7} from 260 to 1500 K.

"heavy likes heavy" rule also applies to the M^{2+} cations in carbonates, albeit weakly. The experimentally observed *inverse* relationship between the atomic number of the M^{2+} cation and affinity for heavy carbon and oxygen isotopes thus cannot be a direct mass effect, but is instead caused by other chemical properties that correlate with atomic number. The most likely properties are ionic radius and

Table 8
Estimates of equilibrium $^{13}C/^{12}C$ and $^{18}O/^{16}O$ fractionation factors for carbonate minerals

Mineral	Number wave vectors (phonons) sampled	0 °C		25 °C		100 °C		300 °C		1000 °C	
		α_{MCO_3-C}	α_{MCO_3-O}	α_{MCO_3-C}	α_{MCO_3-O}	α_{MCO_3-C}	α_{MCO_3-O}	α_{MCO_3-C}	α_{MCO_3-O}	α_{MCO_3-C}	α_{MCO_3-O}
Calcite	1 (30)	1.22942	1.11822	1.19974	1.10222	1.13870	1.06973	1.06605	1.03225	1.01469	1.00699
	2 (60)	1.23398	1.11873	1.20383	1.10267	1.14179	1.07005	1.06776	1.03243	1.01513	1.00703
	5 (150)	**1.23450**	**1.11942**	**1.20430**	**1.10328**	**1.14215**	**1.07051**	**1.06797**	**1.03268**	**1.01519**	**1.00710**
Dolomite	1 (30)	1.23302	1.12390	1.20292	1.10706	1.14099	1.07294	1.06723	1.03370	1.01498	1.00730
	2 (60)	**1.23783**	**1.12470**	**1.20722**	**1.10775**	**1.14423**	**1.07341**	**1.06904**	**1.03394**	**1.01545**	**1.00736**
Magnesite	1 (30)	1.23573	1.12995	1.20529	1.11219	1.14269	1.07628	1.06809	1.03516	1.01518	1.00760
	2 (60)	**1.24174**	**1.13231**	**1.21065**	**1.11425**	**1.14670**	**1.07775**	**1.07032**	**1.03593**	**1.01576**	**1.00779**
Aragonite	1 (60)	*1.23723*	*1.11927*	*1.20673*	*1.10322*	*1.14394*	*1.07058*	*1.06894*	*1.03280*	*1.01543*	*1.00714*
	2 (120)	***1.23718***	***1.11923***	***1.20669***	***1.10319***	***1.14391***	***1.07056***	***1.06892***	***1.03279***	***1.01543***	***1.00714***
Witherite	1 (60)	***1.22961***	***1.11365***	***1.20000***	***1.09835***	***1.13904***	***1.06721***	***1.06634***	***1.03117***	***1.01479***	***1.00677***
Nahcolite	1 (72)	***1.23042***	***1.12658***	***1.20088***	***1.10980***	***1.14006***	***1.07561***	***1.06734***	***1.03571***	***1.01518***	***1.00798***

α_{MCO_3-C} is the ratio $(^{13}C/^{12}C)_{MCO3}/(^{13}C/^{12}C)_C$, where "C" refers to a monoatomic carbon gas, and α_{MCO_3-O} is the ratio $(^{18}O/^{16}O)_{MCO_3}/(^{18}O/^{16}O)_O$, where "O" refers to a monoatomic oxygen gas. Italicized entries indicate data averaged over two or more crystallographically distinct sites. Bold type entries indicate best-estimate model result.

Table 9
Polynomial fits to calculated equilibrium carbon and oxygen fractionation factors

	E	F	G	H
α_{MCO_3-C}				
Calcite [$CaCO_3$]	-1.02673×10^{18}	4.83879×10^{13}	-1.02699×10^{9}	2.50497×10^{4}
Dolomite [$MgCa(CO_3)_2$]	-1.07142×10^{18}	5.02619×10^{13}	-1.05752×10^{9}	2.54790×10^{4}
Magnesite [$MgCO_3$]	-1.12741×10^{18}	5.26094×10^{13}	-1.09579×10^{9}	2.59972×10^{4}
Aragonite [$CaCO_3$]	-1.07631×10^{18}	5.04470×10^{13}	-1.06032×10^{9}	2.54463×10^{4}
Witherite [$BaCO_3$]	-9.53983×10^{17}	4.53364×10^{13}	-9.77236×10^{8}	2.43900×10^{4}
Nahcolite [$NaHCO_3$]	-1.18120×10^{18}	5.40181×10^{13}	-1.09396×10^{9}	2.50058×10^{4}
α_{MCO_3-O}				
Calcite [$CaCO_3$]	-2.85337×10^{17}	1.42104×10^{13}	-3.44477×10^{8}	1.16634×10^{4}
Dolomite [$MgCa(CO_3)_2$]	-2.88192×10^{17}	1.43658×10^{13}	-3.48365×10^{8}	1.20888×10^{4}
Magnesite [$MgCO_3$]	-3.20756×10^{17}	1.57419×10^{13}	-3.71753×10^{8}	1.28014×10^{4}
Aragonite [$CaCO_3$]	-3.05840×10^{17}	1.50777×10^{13}	-3.58924×10^{8}	1.17372×10^{4}
Witherite [$BaCO_3$]	-2.686055×10^{17}	1.34516×10^{13}	-3.29688×10^{8}	1.11306×10^{4}
Nahcolite [$NaHCO_3$]	-5.68538×10^{17}	2.52758×10^{13}	-5.06817×10^{8}	1.30720×10^{4}

Each fit has the form: $\alpha = E/T^8 + F/T^6 + G/T^4 + H/T^2 + 1$. These reproduce equilibrium $^{13}C/^{12}C$ fractionations within 0.16‰ above 260 K, and $^{18}O/^{16}O$ fractionations within 0.11‰ over the same temperature range.

Table 10
Calculated $^{13}C/^{12}C$ and $^{18}O/^{16}O$ fractionation factors for ^{40}Mg—magnesite and ^{40}Ba—witherite at 25 °C

Mineral	Number of wave vectors (phonons) sampled	25 °C	
		α_{MCO_3-C}	α_{MCO_3-O}
^{40}Mg—magnesite	2 (60)	**1.21074**	**1.11428**
^{40}Ba—witherite	1 (60)	**1.19994**	**1.09833**

chemical hardness. Bigeleisen and Mayer (1947) showed that isotopic fractionation is dominantly controlled by inter-atomic force constants for most materials at temperatures above 0 °C. Heavy elements, which tend to have larger ionic radii and easily deformed electronic structures, are expected and observed to form chemical bonds with lower force constants than otherwise similar bonds involving light elements. Ba^{2+}–O bonds in witherite are 2.7–2.9 Å in length, while the Ca^{2+}–O bonds in structurally similar aragonite are ~0.2–0.3 Å shorter. Mg^{2+}–O bonds in magnesite and dolomite are likewise ~0.25 Å shorter than Ca^{2+}–O bonds in calcite. Cadmium in the mineral otavite ($CdCO_3$) has roughly the same 2+ ionic radius as calcium. However, high atomic-number elements like cadmium also have more easily deformed valence orbital structures, as indicated by the strong tendency of cadmium to form sulfides. In each instance, the high atomic-number element is expected to form longer or more plastic M^{2+}–O bonds with lower force constants than lower atomic-number elements, consistent with the trends observed in $^{13}C/^{12}C$ and $^{18}O/^{16}O$ fractionation factors. These bond-length and deformability trends with increasing atomic number overcome a weak cation-mass effect in the opposite direction.

4. Conclusions

We have determined equilibrium constants for the internal isotopic exchange reaction:

$$M^{12}C^{18}O^{16}O_2 + M^{13}C^{16}O_3 \leftrightarrow M^{13}C^{18}O^{16}O_2 + M^{12}C^{16}O_3$$

where M is Ca (calcite, aragonite, and dolomite), Mg (magnesite and dolomite), Ba (witherite), Na and H (nahcolite), as well as the similar reaction:

$$Ca^{12}C^{18}O^{16}O_2 + Ca^{12}C^{17}O^{16}O_2 \leftrightarrow Ca^{12}C^{18}O^{17}O^{16}O + Ca^{12}C^{16}O_3$$

in calcite using first-principles lattice dynamics. The results suggest that there will be an ~0.4‰ excess of $^{13}C^{18}O^{16}O_2{}^{2-}$ groups in all studied carbonate minerals at room-temperature equilibrium, relative to the abundance expected in a stochastic mixture of carbon and oxygen isotopes in the crystal lattice. There will also be a ~0.1‰ excess of $^{12}C^{18}O^{17}O^{16}O^{2-}$ at the same temperature. Both excesses decrease with increasing temperature, and are roughly linear vs. $1/T^2$ from 0 to 300 °C, suggesting that accurate measurements could be used to estimate carbonate mineral crystallization temperatures. The predicted temperature sensitivity of K_{eq}[3866] is ~0.003‰/°C at 25 °C. Mass-47 CO_2 derived from conventional phosphoric acid digestion of carbonates will largely be controlled by the $^{13}C^{18}O^{16}O_2{}^{2-}$ abundance (~96% at typical terrestrial $^{13}C/^{12}C$, $^{17}O/^{16}O$, and $^{18}O/^{16}O$), with $^{12}C^{18}O^{17}O^{16}O^{2-}$ contributing most of the remainder (3%). Thus, the carbonate internal equilibration temperatures are likely to be detectable from gas-phase isotope-ratio mass-spectrometric measurements of excess mass-47 CO_2.

Crystal chemistry appears to have little effect on estimated equilibrium constants for the formation of $^{13}C^{18}O^{16}O_2{}^{2-}$, and the small variations between different carbonate minerals generally appear to follow the same systematics as $^{13}C/^{12}C$ and $^{18}O/^{16}O$ fractionation, with larger $^{13}C^{18}O^{16}O_2{}^{2-}$ excesses and higher $^{13}C/^{12}C$ and $^{18}O/^{16}O$ ratios expected in Mg-bearing carbonates than Ca- or Ba-bearing carbonates, and in orthorhombic vs. rhombohedral carbonates.

Comparisons of model vibrational spectra of ^{18}O-substituted calcite with measured spectra (Gillet et al., 1996), and between model and observed $^{13}C/^{12}C$ and $^{18}O/^{16}O$ fractionations suggest uncertainties of order $2–3 \times 10^{-5}$ in calculated equilibrium constants. The density functional perturbation theory (DFPT) method used to estimate phonon frequencies appears to accurately reproduce measured frequencies (rms error of 10 cm^{-1} after scaling for anhydrous carbonates) and stable isotope fractionations (within ~1–2‰ at 25 °C). Interestingly, C- and O-isotope fractionation results in hypothetical ^{40}Mg—magnesite and ^{40}Ba—witherite indicate that M^{2+}-cation mass does not contribute significantly to isotopic fractionations between carbonate minerals.

Acknowledgments

This work is supported by the National Science Foundation, including grant EAR-0345433 to E.A.S. and a period two technician support grant to P.G. and J.M.E., and by a Packard Fellowship to J.M.E. We thank Juske Horita and an anonymous reviewer for thoughtful and constructive reviews of this work. Discussions with Weifu Guo about stable-isotope fractionation and ^{13}C–^{18}O clumping effects were particularly helpful during the initial preparation of this manuscript.

Associate editor: Juske Horita

Appendix A. Scale factors and model accuracy

The main causes of uncertainty in estimated equilibrium constants for the formation of ^{13}C–^{18}O-bearing carbonate isotopologues probably stem from errors in model (DFPT) phonon frequencies. Measurements of phonon frequencies in isotopically substituted carbonate minerals are sparse, so the best way to check the accuracy of our model results is by comparing DFPT models with the more extensive Raman, infrared, and neutron-scattering results on isotopically normal crystals.

Unfortunately, it is not always obvious which model frequency corresponds to a particular absorption band or Raman spectral feature. This appendix describes the methods we used to correlate model frequencies with observations. The correlations indicate that our DFPT models systematically underestimate measured frequencies by ~3% (Table 3), suggesting that model accuracies are improved by the addition of a modest scale factor. For the minerals calcite, magnesite, dolomite, aragonite and witherite, we are able to correlate a total of 100 measured phonon frequencies with model frequencies. Taken together, these suggest a uniform scale factor of 1.0331 with an rms misfit of 10 cm^{-1}. Nahcolite appears to have a significantly different scale factor of 1.0154, with an rms misfit of 19 cm^{-1}. It is not clear if this difference reflects a less accurate model with distinct systematic frequency errors, or the lack of precise single-crystal infrared and Raman spectroscopic studies of this mineral. The presence of O–H bonds, which typically show significant vibrational anharmonicity, may also cause some of the difference.

In the discussion and table below we report scaled model results. This simplifies comparisons between observed and model frequencies, at the cost of some circularity of reasoning.

A.1. Rhombohedral carbonates (calcite, magnesite, and dolomite)

High-quality single-crystal infrared and Raman spectral studies of the rhombohedral carbonates calcite, dolomite and magnesite are available in the literature (e.g., Porto, 1966; Hellwege et al., 1970; Rutt and Nicola, 1974; Nicola et al., 1976). One neutron scattering study also examined low-frequency phonons in calcite (Cowley and Pant, 1973). We have used these measurements to check model calculations on isotopically normal crystals (by normal we mean that each atom of an element is assumed to have the average atomic mass of that element). Model and observed frequencies are correlated on the basis of their symmetry species and rank from highest frequency to lowest frequency (e.g., the highest frequency E_g mode in our calcite model is correlated with the highest frequency E_g mode observed). Dolomite requires some additional care because a few nominally infrared- and Raman-active modes are so weak that they do not show up in experiments. DFPT calculations indicate that the mode at 1105 cm^{-1} interacts much more weakly with infrared light than the other modes with A_u symmetry, so we have not tried to correlate it with observed spectral features. There are also two nominally Raman-active A_g modes in dolomite, at 876 and 231 cm^{-1}, that are related to Raman-inactive A_{2g} modes in $R\bar{3}c$ carbonates like calcite. These appear to be too weak to be distinguished from noise under experimental conditions, and we have not attempted to correlate them either.

For calcite we correlated 22 measured and model frequencies of zero wave-vector phonons, relying mainly on the tabulation of Pilati et al. (1998) for Raman, infrared, and neutron-scattering results. These suggest an excellent match between our model and observed phonon frequencies (Fig. 2), with a scale factor of 1.033 and a root-mean-square (rms) misfit of 11 cm^{-1}. With magnesite we correlated 21 measured phonon frequencies (Rutt and Nicola, 1974) with model results, and calculated a scale factor of 1.032 with an rms misfit of 8 cm^{-1}. We also estimate a scale factor of 1.035 for dolomite based on the 23 measured frequencies tabulated in Pilati et al., 1998, and an rms error of 8 cm^{-1}. The estimated scale factors and rms errors for all three models are remarkably uniform; individual scale factors are all within one standard error of the aggregate scale factor of 1.0331.

A.2. Orthorhombic and monoclinic carbonates (aragonite, witherite, and nahcolite)

A.2.1. Aragonite ($CaCO_3$)

Aragonite has been the subject of careful infrared and Raman spectroscopy studies (Frech et al., 1980; Martens et al., 2004), but the zero wave-vector frequencies for this mineral are still incompletely known. This makes it more difficult to rigorously compare model and experimental results.

The nine expected vibrational modes of A_g-symmetry, which are Raman-active, were all identified by Frech et al. (1980). These we have matched with model results in frequency order, suggesting a scale factor of ~1.03. These authors were also able to identify all but the highest-frequency modes of B_{3g} symmetry in their Raman spectra; the model result for this high-frequency mode is 1418 cm^{-1} after applying the aggregate 1.0331 scale factor. Since all the other B_{3g} modes have frequencies less than $\frac{1}{2}$ as large, we are confident in correlating the model and observed modes of this symmetry species. Frequency measurements of phonons with B_{1g} and B_{2g} symmetry, which are all nominally Raman-active, are too incomplete for us to correlate to model results with confidence.

Frech et al. (1980) also measured infrared reflection spectra between 680 and 1600 cm^{-1}. The strongest infrared bands predicted by the model (TO modes) are at 1476 cm^{-1} (B_{1u}) and 1448 cm^{-1} (B_{2u}) after scaling. These closely match strong reflectivity features observed at 1466 and 1443 cm^{-1}, respectively. The strongest infrared-active model modes in the 800–1100 cm^{-1} range are at 1095 cm^{-1} (B_{1u}), 1094 cm^{-1} (B_{3u}), and 857 cm^{-1} (B_{3u}), matching observed bands at 1085 cm^{-1}, 1083 cm^{-1}, and 853 cm^{-1}. At frequencies below 800 cm^{-1}, the model modes with the strongest calculated infrared intensities are at 709 cm^{-1} (B_{1u}) and 697 cm^{-1} (B_{2u}). These also correlate well with observed modes at 713 and 699 cm^{-1}.

Together, all 21 correlated model and observed frequencies for aragonite suggest a mineral-specific scale factor of

1.0299, and an rms misfit of 12 cm^{-1}. This is one standard error lower than the aggregate scale factor.

A.2.2. Witherite ($BaCO_3$)

We are aware of only one attempt to measure and classify vibrational frequencies in witherite according to their symmetry species (Martens et al., 2004). That study proposed a handful of symmetry and frequency assignments for Raman active modes, including the four highest-frequency A_g modes, two B_{2g} modes, two B_{1g} modes and one B_{3g} mode. The four Ag modes can be correlated unambiguously with model results, suggesting a scale factor of approximately 1.03. Our model results for other Raman-active modes are in good agreement for all but the three highest-frequency modes Exp.: B_{3g}—1539 cm^{-1}, B_{1g}—1509 cm^{-1} and B_{2g}—1450 cm^{-1}. Model: 1404, 1429, and 1518 cm^{-1}, respectively. We suspect that these modes may have been assigned to the wrong symmetry group, because the highest frequency model B_{2g} mode (1518 cm^{-1} after scaling) is much closer to the measured "B_{1g}" and "B_{3g}" frequencies, but this remains a point of uncertainty.

In the absence of polarized single-crystal infrared studies of witherite, we have matched measured infrared absorption features observed in powdered samples (Pasierb et al., 2001) to model frequencies on the basis of oscillator intensities calculated with DFPT. The DFPT results indicate that there are six vibrational modes between 200 and 1600 cm^{-1} with oscillator strengths greater than an arbitrary threshold of 2.5×10^{-6} m^3/s^2 (B_{1u}—1427 cm^{-1}, B_{2u}—1424 cm^{-1}, B_{1u}—1072 cm^{-1}, B_{3u}—861 cm^{-1}, B_{1u}—694 cm^{-1} and B_{2u}—692 cm^{-1} after scaling). All other modes in this frequency range are at least 30× fainter. It seems reasonable to expect that the first two modes will combine to make a single absorption feature in powder spectra, as will the two low-frequency modes, yielding a spectrum with four prominent absorbance peaks. These peaks and frequencies are in excellent agreement with the four absorbance peaks observed (Pasierb et al., 2001).

In total, we are able to correlate twelve model phonon frequencies with observed spectral features. The best-fit scale factor for these data is 1.036, with an rms misfit of 13 cm^{-1}. This scale factor is within one standard error of the aggregate scale factor.

A.2.3. Nahcolite ($NaHCO_3$)

Raman and infrared spectra of nahcolite have been measured in powder and a Nujol mull (Bertoluzza et al., 1981). These measurements do not permit the assignment of observed bands to particular symmetry species, complicating the comparison of observed and modeled frequencies. As with witherite, we correlate measured infrared absorption features with calculated phonon frequencies by trying to match calculated oscillator strengths with observed absorption strengths. Model calculations suggest that there are two IR-active modes in the O–H stretching region (2669 and 2534 cm^{-1}), with the 2534 cm^{-1} mode 10× stronger, while measurements (Bertoluzza et al., 1981) find one strong absorption band at 2542 cm^{-1}, one medium-strength mode at 2450 cm^{-1}, and one weak mode at 2650 cm^{-1}. We tentatively correlate the 2534 cm^{-1} model frequency with the strong 2542 cm^{-1} band. This suggests a correlation between the 2669 cm^{-1} band and the observed 2650 cm^{-1} band, but this is uncertain.

There are six model modes between 1200 and 1700 cm^{-1} with significant predicted infrared absorptivity, at 1643, 1618, 1470, 1449, 1410, and 1270 cm^{-1}. Bertoluzza et al. (1981) find six very strong, strong, and medium-strength modes in the same frequency range. We correlate the very-strong 1300 cm^{-1} band of Bertoluzza et al. (1981) with the strongest model mode at 1270 cm^{-1}. The other strong absorption bands observed at 1655, 1617, 1452, and 1398 cm^{-1} are tentatively correlated with model frequencies at 1643, 1617, 1470, and 1409 cm^{-1}. The model 1449 cm^{-1} mode, with <15% of the predicted infrared activity of the other modes, may be too weak to show up in a powder spectrum.

Bertoluzza et al. (1981) also find eight infrared absorption bands between 200 and 1100 cm^{-1} (1045 cm^{-1} medium, 1032 cm^{-1} strong, 997 cm^{-1} strong, 836 cm^{-1} very strong, 812 cm^{-1} shoulder, 694 cm^{-1} very strong, 656 cm^{-1} strong, and 255 cm^{-1} medium). The strongest model frequencies in this range are at 1079, 1031, 1008, 822, 689, 652, 231, 223, and 214 cm^{-1}. The strongest absorption band at 694 cm^{-1} matches up well with the strongest model frequency at 689 cm^{-1}. However, there is no obvious model counterpart for the observed 836 cm^{-1} band—the closest mode at 822 cm^{-1} is predicted to be only 10% as strong as the 679 cm^{-1} band, and significantly weaker than several other modes in the <1000 cm^{-1} frequency interval, suggesting a better correlation with the observed 812 cm^{-1} band. The three model modes between 214 and 231 cm^{-1} may well not be distinguishable in the powder spectrum, and most likely correlate with the observed 255 cm^{-1} band. For the purpose of determining a scale factor, we correlate this band with the 223 cm^{-1} mode, which is predicted to be twice as intense as the other two combined. The other modes are correlated in frequency order.

Although Bertoluzza et al. (1981) identified numerous Raman features in their study, we could only correlate the 1047 cm^{-1} mode with any confidence. The model A_{1g} mode at 1031 cm^{-1} is the symmetric v_1 vibration of the carbonate ion, with all four HCO_3^- groups in the unit cell vibrating in phase. This characteristic motion is consistent with the very strong observed Raman scattering.

In estimating a scale factor relating model and observed phonon frequencies for nahcolite we have ignored O–H stretching and bending modes at 2650, 2542, and 997 cm^{-1}. $NaHCO_3$ has relatively strong hydrogen bonds, and the O–H modes in such a system are likely to show substantial anharmonicity. Zero-point energy contributions from O–H stretching and bending frequencies are thus likely to be underestimated by measured frequencies. A proportional best fit through the other frequencies suggests a scale factor of 1.0145, slightly smaller than was

found for the anhydrous carbonates. The rms misfit of the twelve correlated modes is 19 cm^{-1}, somewhat worse than the other models. This could reflect difficulties in matching model frequencies with observations, a poorer quality of model, or non-linear scaling behavior for modes with significant (if not dominant) O–H bond distortions.

References

Affek, H.P., Eiler, J.M., 2006. Abundance of mass 47 CO_2 in urban air, car exhaust, and human breath. *Geochim. Cosmochim. Acta* **70**, 1–12.

Angus, W.R., Bailey, C.R., Hale, J.B., Ingold, C.K., Leckie, A.H., Raisin, C.G., Thompson, J.W., Wilson, C.L., 1936. Structure of benzene. Part VIII. Assignment of vibrational frequencies of benzene and hexadeuterobenzene. *J. Chem. Soc. (London)*, 971–987.

Bechtel, A., Hoernes, S., 1990. Oxygen isotope fractionation between oxygen of different sites in illite minerals—a potential single-mineral thermometer. *Contrib. Mineral. Petrol.* **104**, 463–470.

Bertoluzza, A., Monti, P., Morelli, M.A., Battaglia, M.A., 1981. A Raman and infrared spectroscopic study of compounds characterized by strong hydrogen bonds. *J. Mol. Struct.* **73**, 19–29.

Bigeleisen, J., Mayer, M.G., 1947. Calculation of equilibrium constants for isotopic exchange reactions. *J. Chem. Phys.* **15**, 261–267.

Chacko, T., Cole, D.R., Horita, J., 2001. Equilibrium oxygen, hydrogen and carbon isotope fractionation factors applicable to geologic systems. In: Valley, J.W., Cole, D.R. (Eds.), *Stable Isotope Geochemistry. Rev. Mineral. Geochem.* 43, pp. 1–81.

Chacko, T., Mayeda, T.K., Clayton, R.N., Goldsmith, J.R., 1991. Oxygen and carbon isotope fractionations between CO_2 and calcite. *Geochim. Cosmochim. Acta* **55**, 2867–2882.

Cowley, E.R., Pant, A.K., 1973. Lattice dynamics of calcite. *Phys. Rev. B* **8**, 4795–4800.

Deines, P., 2004. Carbon isotope effects in carbonate systems. *Geochim. Cosmochim. Acta* **68**, 2659–2679.

Eiler, J.M., Schauble, E.A., 2004. $^{18}O^{13}C^{16}O$ in earth's atmosphere. *Geochim. Cosmochim. Acta* **68**, 4767–4777.

Emrich, K., Ehalt, D.H., Vogel, J.C., 1970. Carbon isotope fractionation during the precipitation of calcium carbonate. *Earth Planet. Sci. Lett.* **8**, 363–371.

Epstein, S., Buchsbaum, R., Lowenstam, H.A., Urey, H.C., 1953. Revised carbonate–water isotopic temperature scale. *Geol. Soc. Am. Bull.* **64**, 1315–1326.

Filippi, C., Singh, D.J., Umrigar, C.J., 1994. All-electron local-density and generalized-gradient calculations of the structural properties of semiconductors. *Phys. Rev. B* **50**, 14947–14951.

Frech, R., Wang, E.C., Bates, J.B., 1980. The IR, Raman spectra of $CaCO_3$ (aragonite). *Spectrochim. Acta* **36A**, 915–919.

Friedman, I., O'Neil, J.R., 1977. *Compilation of Stable Isotope Fractionation Factors of Geochemical Interest*. USGS Prof. Paper 440-KK.

Graf, D.L., 1961. Crystallographic tables for the rhombohedral carbonates. *Am. Mineral.* **46**, 1283–1316.

Ghosh, P., Adkins, J., Affek, H., Balta, B., Guo, W., Schauble, E.A., Shrag, D., Eiler, J.M., 2006. ^{13}C–^{18}O bonds in carbonate minerals: a new kind of paleothermometer. *Geochmim. Cosmochim. Acta* **70**, 1439–1456.

Gillet, P., McMillan, P., Schott, J., Badro, J., Grzechnik, A., 1996. Thermodynamic properties and isotopic fractionation of calcite from vibrational spectroscopy of ^{18}O-substituted calcite. *Geochim. Cosmochim. Acta* **60**, 3471–3485.

Gillet, P., Biellmann, C., Reynard, B., McMillan, P.F., 1993. Raman spectroscopic studies of carbonates. Part I: High-pressure and high-temperature behaviour of calcite, magnesite, dolomite, and aragonite. *Phys. Chem. Minerals* **20**, 1–18.

Golyshev, S.I., Padalko, N.L., Pechenkin, S.A., 1981. Fractionation of stable oxygen and carbon isotopes in carbonate systems. *Geochem. Int.* **18**, 85–99.

Gonze, X., Beuken, J.-M., Caracas, R., Detraux, F., Fuchs, M., Rignanese, G.M., Sindic, L., Verstraete, M., Zerah, G., Jollet, F., Torrent, M., Roy, A., Mikami, M., Ghosez, P., Raty, J.Y., Allan, D.C., 2002. First-principles computation of material properties: the ABINIT software project. *Comp. Mat. Sci.* **25**, 478–492.

Gonze, X., Stumpf, R., Scheffler, M., 1991. Analysis of separable pseudopotentials. *Phys. Rev. B* **44**, 8503–8513.

Grossman, E.L., Ku, T.-L., 1986. Oxygen and carbon isotope fractionation in biogenic aragonite: temperature effects. *Chem. Geol.* **59**, 59–74.

Hamza, M.S., Epstein, S., 1980. Oxygen isotopic fractionation between oxygen of different sites in hydroxyl-bearing silicate minerals. *Geochim. Cosmochim. Acta* **44**, 173–182.

Hellwege, K.H., Lesch, W., Plihal, M., Schaack, G., 1970. Zwei-Phononen-Absorptionsspektren end dispersion der Schwingungszweige in Kristallen der Kalkspatstruktur (Translated title: "Two phonon absorption spectra and dispersion of phonon branches in crystals of calcite structure"). *Z. Physik* **232**, 61–86.

Kieffer, S.W., 1982. Thermodynamics and lattice vibrations of minerals. 5. Application to phase equilibria, isotopic fractionation and high-pressure thermodynamic properties. *Rev. Geophys. Space Phys.* **20**, 827–849.

Kim, S.-T., O'Neil, J.R., 1997. Equilibrium and nonequilibrium oxygen isotope effects in synthetic carbonates. *Geochim. Cosmochim. Acta* **61**, 3461–3475.

Lee, C., Vanderbilt, D., Laasonen, K., Car, R., Parrinello, M., 1992. Abinitio studies on high pressure phases of ice. *Phys. Rev. Lett.* **69**, 462–465.

Louie, S.G., Froyen, S., Cohen, M.L., 1982. Nonlinear ionic pseudopotentials in spin-density-functional calculations. *Phys. Rev. B* **26**, 1738–1742.

Martens, W.N., Rintoul, L., Kloprogge, J.T., Frost, R.L., 2004. Single crystal Raman spectroscopy of cerussite. *Am. Mineral.* **89**, 352–358.

Matthews, A., Katz, A., 1977. Oxygen isotope fractionation during the dolomitization of calcium carbonate. *Geochim. Cosmochim. Acta* **41**, 1431–1438.

Nicola, J.H., Scott, J.F., Couto, R.M., Correa, M.M., 1976. Raman spectra of dolomite [$CaMg(CO_3)_2$]. *Phys. Rev. B* **14**, 14–16.

Northrop, D.A., Clayton, R.N., 1966. Oxygen-isotope fractionations in systems containing dolomite. *J. Geol.* **74**, 174–196.

Parrington, J.R., Knox, H.D., Breneman, S.L., Baum, E.M., Feiner, F., 1996. *Chart of the Nuclides*. General Electric Co. and KAPL Inc.

Pasierb, P., Komornicki, S., Rokita, M., Rekas, M., 2001. Structural properties of Li_2CO_3–$BaCO_3$ system derived from IR and Raman spectroscopy. *J. Mol. Struct.* **596**, 151–156.

Patterson, W.P., Smith, G.R., Lohmann, K.C., 1993. Continental paleothermometry and seasonality using the isotopic composition of aragonitic otoliths of freshwater fishes. In: Swart, P.K., et al. (Ed.), Climate Change in Continental Isotopic Records, *Geophys. Monogr. Ser.* 78, 191–202.

Perdew, J.P., Zunger, A., 1981. Self-interaction correction to density-functional approximations for many-electron systems. *Phys. Rev. B.* **23**, 5048–5079.

Perdew, J.P., Burke, K., Ernzerhof, M., 1996. Generalized gradient approximation made simple. *Phys. Rev. Lett.* **77**, 3865–3868.

Pilati, T., Demartin, F., Gramaccioloi, C.M., 1998. Lattice-dynamical estimation of atomic displacement parameters in carbonates: calcite and aragonite $CaCO_3$, dolomite $CaMg(CO_3)_2$ and magnesite $MgCO_3$. *Acta Cryst. B* **54**, 515–523.

Porto, S.P.S., 1966. Depolarization of Raman scattering in calcite. *Phys. Rev.* **147**, 608–611.

Prencipe, M., Pascale, F., Zicovich-Wilson, C.M., Saunders, V.R., Orlando, R., Dovesi, R., 2004. The vibrational spectrum of calcite ($CaCO_3$): an ab initio quantum-mechanical calculation. *Phys. Chem. Minerals* **31**, 559–564.

Rappe, A.M., Rabe, K.M., Kaxiras, E., Joannopoulos, J.D., 1990. Optimized pseudopotentials. *Phys. Rev. B* **41**, 1227–1230.

Romanek, C.S., Grossman, E.L., Morse, J.W., 1992. Carbon isotopic fractionation in synthetic aragonite and calcite: effects of temperature and precipitation rate. *Geochim. Cosmochim. Acta* **56**, 419–430.

Rosenbaum, J.M., 1997. Gaseous, liquid, and supercritical fluid H_2O and CO_2: oxygen isotope fractionation behavior. *Geochim. Cosmochim. Acta* **61**, 4993–5003.

Ross, N.L., 1997. The equation of state and high-pressure behavior of magnesite. *Am. Mineral.* **82**, 682–688.

Ross, N.L., Reeder, R.J., 1992. High-pressure structural study of dolomite and ankerite. *Am. Mineral.* **77**, 412–421.

Rubinson, M., Clayton, R.N., 1969. Carbon-13 fractionation between aragonite and calcite. *Geochim. Cosmochim. Acta* **33**, 997–1002.

Rutt, H.N., Nicola, J.H., 1974. Raman spectra of carbonates of calcite structure. *J. Phys. C* **7**, 4522–4528.

Sauss, R.L., Scheuerman, R.F., 1962. The crystal structure of sodium bicarbonate. *Acta Cryst.* **15**, 77–81.

Sharma, B.D., 1965. Sodium bicarbonate and its hydrogen atom. *Acta Cryst.* **18**, 818–819.

Sheppard, S.M.F., Schwarcz, H.P., 1970. Fractionation of carbon and oxygen isotopes and magnesium between coexisting metamorphic calcite and dolomite. *Contrib. Mineral. Petrol.* **26**, 161–198.

Sommer, M.A., Rye, D., 1978. *Oxygen and Carbon Isotope Internal Thermometry Using Benthic Calcite and Aragonite Foraminifera Pairs. Short Papers, 4th Int'l Conf. Geochron. Cosmochron. Isotope Geol., USGS Open File Rept.* 78-701, pp. 408–410.

Tarutani, T., Clayton, R.N., Mayeda, T.K., 1969. The effect of polymorphism and magnesium substitution on oxygen isotope fractionation between calcium carbonate and water. *Geochim. Cosmochim. Acta* **33**, 987–996.

Urey, H.C., 1947. The thermodynamic properties of isotopic substances. *J. Chem. Soc. (Lond.)*, 562–581.

de Villiers, J.P.R., 1971. Crystal structures of aragonite, strontianite, and witherite. *Am. Mineral.* **56**, 758–767.

Wang, Z., Schauble, E.A., Eiler, J.M., 2004. Equilibrium thermodynamics of multiply substituted isotopologues of molecular gases. *Geochim. Cosmochim. Acta* **68**, 4779–4797.

Wilson, E.B.J., Decius, J.C., Cross, P.C., 1955. *Molecular Vibrations: The Theory of Infrared and Raman Vibrational Spectra*. Dover, New York.